International Journal of Environment
Volume: 13 | Issue: 01| Jan. - March| 2024

EISSN: 2706-7939 ISSN: 2077-4508
DOI: 10.36632/ije/2024.13.1.1
Journal homepage: www.curresweb.com
Pages: 1-26

Study The Negative Effect of the Accumulation of Iron and Manganese Ions in Groundwater Irrigation with Treatment by Magnetic Nanomaterials and Its Relationship of Surface and Subsurface Soils Characteristics

Yasser A. M. Abdulhady[1] and Ahmed S. A. Sayed[2]

[1]Hydro geochemistry Department, Desert Research Center, Water Treatment and Desalination, El-Mataryia, Cairo, Egypt.
[2]Pedology Department, Desert Research Center, El –Mataryia, Cairo, Egypt.

Received: 30 Nov. 2023 **Accepted: 30** Jan. 2024 **Published: 20** Feb. 2024

ABSTRACT
The article's goal was to examine the treatment of contaminated groundwater and its connection to soil characterization. The production of crops was negatively impacted by the accumulation of iron metal in soil and groundwater, necessitating treatment and crop selection. Titania-coated cobalt ferrite nanocomposite for treating contaminated groundwater was created using the sol gel technique. Particle size distribution, BET, FTIR, SEM, XRD, VSM, and EDX techniques were used to characterize the prepared nanocomposite. The solution's pH, contact time, amount of adsorbent, initial ion concentration, and temperature were all examined. Fe (II) and Mn (II) ion maximum adsorption capacities ranged from 83% to 94% mg/g once the ideal adsorption conditions were identified and applied. When reclaiming our lands, it is important to assess the soil resources to determine whether the land is suitable for growing crops. In the Dakhla-Abu Minqar District, Western Desert, Egypt, soil properties are assessed and analyzed for the majority of irrigated crops; land capability and suitability for crops maps are created using the Geographic Information System. The Geographic Information System (GIS) is used to create land suitability maps, and the majority of irrigated according to Applied System of Land Evaluation (ASLE) program, and evaluation of their soil properties. The study's findings showed that the area is currently land capability fair (Class 3) to very poor soils (C5), while suitable (S2) and marginally suitable (S4) for permanent and semi-annual crops. Soil depth, soil salinity, drainage, and texture were the primary constraints found in the soils.

Keywords: groundwater treatment, Titania-coated cobalt ferrite nanocomposite, Iron & Manganese Removal, soil properties, crop suitability

1. Introduction

The bedrock composition of the aquifer through which groundwater flows has a major impact on its chemistry. The hydro chemical processes and hydrogeology of groundwater vary spatially and temporally, depending on the geology and chemical composition of the aquifer. Groundwater's chemical composition can be controlled by hydrogeological processes like dissolution, precipitation, ion exchange processes, and time with flow path (Apodaca *et al.,* 2002). Groundwater has become the primary source of water supply due to the increasing population and rapid urbanization. Studying the quality of groundwater and the processes that control the concentration of major constituents in the area is now necessary (Amadi *et al.,* 1989; Udom *et al.,* 1999; Nwankwoala *et al.,* 2007 and Foster w*et al.,* 2003). The complexity and location of soil-water-pollutant interactions have resulted in the pollution of groundwater; the fate of contaminants in the aquifers is uncertain (Shrestha *et al.,* 2016; Yan *et al.,* 2023; Lin *et al.,* (2023). Groundwater management must prioritize pollution prevention and control as a crucial component. Iron is a common trace element in soils and groundwater. Iron is the fourth most abundant mineral in the earth's crust. (Xiao *et al.,* 2023; Pan *et al.,* 2022). The bulk

Corresponding Author: Yasser A. M. Abdulhady, Hydro geochemistry Department, Desert Research Center, Water Treatment and Desalination, El –Mataryia, Cairo, Egypt
E-mail address: yasser_vip6@hotmail.com; ORCID.org/0000-0002-7816-4190

iron content of soils is typically in the range of 0.5% to 5% (by volume), and is dependent upon the source rocks from which the soil was derived, transport mechanisms, and overall geochemical history. Iron occurs naturally in water in soluble form as ferrous iron (bivalent iron: Fe^{+2}) or non-soluble form as ferric iron (trivalent iron: Fe^{+3}) (Song *et al.,* 2023). The agriculture field has recently given magnetic nanoparticles (NPs) a lot of attention due to their advantageous magnetic, optical, and treatment properties at the nanoscale. Since Ni, Co, or Cu is tetrahedral sites of typical bivalent cations in a cubic lattice structure, the magnetic Nano ferrites are generally represented as MFe_2O_4 (Ishaq *et al.,* 2017). Compared to other spinel ferrites, cobalt ferrite has an inverse spinel structure and offers a number of benefits, including good coupling efficiency, high magneto-attractiveness, and low cost. Because of its exceptional physical characteristics—high Curie temperature, large magneto-crystalline anisotropy, high coercivity, good chemical stability, large magneto-strictive coefficient, mechanical hardness, and moderate saturation magnetization—$CoFe_2O_4$ has garnered significant attention (Ahmad *et al.,* 2016; Amir *et al.,* 2013). Co is used as a source of gamma rays for plastic manufacturing, radiation therapy for cancer patients, and sterilizing consumer goods and medical equipment (Shirsath *et al.,* 2016). In addition, Co is used in food irradiation, which can be used to sterilize food, eliminate pathogens, prolong food shelf life, decontaminate fruits and grains, postpone ripening, and slow down the sprouting of foods like potatoes and onions. This process depends on the radiation dose. Within the magnetic ferrite class, cobalt ferrite, or $CoFe_2O_4$ (CFO), is one of the most important ferri-magnets with inverse spinel in terms of commerce (Aghrich *et al.,* 2020). Due to its distinct physical characteristics, which include a large magneto crystalline anisotropy, mechanical hardness, excellent chemical stability, high coercivity, mechanical hardness, large magnetostrictive coefficient, and moderate saturation magnetization, $CoFe_2O_4$ has garnered significant attention. Its crystal orientation has a significant impact on its magnetic properties; it exhibits good electrical insulation (Munawar *et al.,* 2021). Moreover, it has been demonstrated by earlier research that $CoFe_2O_4$ is a magnetic particle and that its magnetic properties increase with increasing Mg and Ni concentrations (Velhal *et al.,* 2015). Substituted cobalt ferrites are used as a binder and magnetic filler in nanocomposites for electromagnetic shielding because they show good chemical stability. Additionally, it is commonly anticipated that rare-earth substituted spinel ferrites will frequently display better electric and magnetic properties in comparison to their pure spinel counterparts (Almessiere *et al.,* 2020). Sol gel technique, Chemical precipitation, membrane filtration, ion exchange, and sorption are all involved in physicochemical methods. Electrocoagulation, electro-deposition, and electro-flotation are all electrochemical processes. Several microorganisms help in biodegradation bleaching, which is taken into account by biological methods (Younes *et al.,* 2021). Of all the methods, adsorption is widely applied because of its simplicity, high effectiveness, and the possibility recycling of adsorbents (El- Maghrabi *et al.,* 2019). Many environmental issues have been addressed recently thanks to the advancements in nanoscience and nanotechnology (Chaudhary *et al.,* 2023). Numerous effective, low-cost, and environmentally friendly nanomaterials have been synthesised, characterized, and applied to eliminate toxic ions from wastewater in recent times (Zhang *et al.,* 2022). Nanostructured adsorbents adsorb heavy metal ions through multiple adsorption mechanisms, including electrostatic interaction, ion exchange, and complex formation. The pH dependence of these mechanisms is due to solution pH influencing the number of active sites on the surface of the nano-adsorbent as well as the chemistry of the treated metal ions. Photo catalysis phenomenon has been observed to remove heavy metal ions by utilizing semiconductor-based nanoadsorbents such as TiO_2, ZnO, and Fe_3O_4 (Naseem *et al.,* 2021). Due to their easy synthesis, low poisoning, eco-friendliness, and high affinity, titanium dioxide (TiO_2) nanoparticles have been reported as good adsorbents for the removal of dyes and heavy metals from wastewaters. (Liang *et al.,* 2022). Although there are advantages mentioned, the agglomeration of titania nanoparticles diminishes its surface area and, consequently, its adsorption capacity. In order to solve the agglomeration issue, titanium nanoparticles need to be coated with other transition metals or metal oxides. The adsorption capability of titanium-based nanocomposites is better than that of individual TiO2 nanoparticles due to their larger surface area (Chen *et al.,* 2023).

Hydrogeological and geoglical settings of in the Dakhla-Abu Minqar District

Soil salinization and waterlogging cause debasement of in the Dakhla-Abu Minqar District. At Farafra Desert Oasis, the hard skillet and over-water system at varying depths are seriously affecting the water table (El Bastawesy *et al.,* 2013). Due to a lack of land use planning, land corruption in the Farafra Desert Oasis is predicted to develop into a real and pervasive natural problem in the coming years. Land corruption is a major problem as a result of the penetration from water system zones. Water system projects carried out without the proper seepage framework have disrupted the equilibrium between groundwater recharge and outflow, resulting in a steady addition of groundwater to the El-Farafra. Investigating the water treatment of heavy metals in contaminated groundwater and its connection to soil characterization in the Farafra Desert Oasis is the main objective of this project. The majority of the water resources used for drinking and irrigation come from groundwater (Wang & Cheng *et al.,* 1999; Martinez-Santos *et al.,* 2005; Zuppi, 2011 and Keesari, 2014). In the past few years, an increase of groundwater usage due to expansion in development activities took place because of increased population as well as water scarcity (Omar & Moussa *et al.,* 2016; Clemens *et al.,* 2020). The El Farafra depression study area is part of the New Valley Governorate, which makes up roughly 44% of Egypt's total land area (official website of New Valley governorate). Springs and shallow and deep production wells, which were utilized in the development of these areas years ago, are the primary sources of water in the El Farafra area. The groundwater regime in the study area is made up of two main aquifer systems: the Nubian Sandstone Aquifer System and the Post Nubian Aquifer System. The PNAS, which includes shale intercalations in some areas and covers the Nubian succession, is represented by the carbonate rocks, which take the form of limestone. This system is composed of the following carbonate formations: Lower-Middle Eocene Nagb Limestone, Lower Eocene Farafra Limestone, Paleocene Garra, Paleocene Tarawan Chalk, and Upper Cretaceous Khoman. For groundwater to be stored and transported, carbonate rocks typically need to be fractured or fissured. Groundwater from the underlying Nubian aquifer system moves vertically through fractures and faults, which is the primary source of recharge for this aquifer system (El-Ghamrawy *et al.,* 2021; Mohamed Magdy *et al.,* 2021).

Geomorphology of in the Dakhla-Abu Minqar District

The El Farafra Depression is a semi-closed basin with escarpments surrounding it on all sides. Geographically speaking, El Farafra Oasis has ground elevations ranging from 50 to 150 meters above mean sea level, with some hills like Gebel Gunna El Bahary and Gebel Gunna El Qebly. In general, the study area's geomorphic units can be separated into the following five units: The Depressions and the El Farafra Plateau (ii) The Scarp: Pediments, which are found in the region surrounding the Minqar Depression, which is southwest of the study area, and at the Sahl Qaraween area, represent the foot of moderately tall scarps (Ali *et al.,* 2004) Figure.1. The Quaternary deposits at the study area's surface, which are composed of sand dunes, playa deposits, and sand sheets, represent the Pleistocene to Holocene age. Deposits that are in the third stage as demonstrated by the following configurations: The Lower to Middle Eocene is the age range of the Nagb Limestone Formation (Tetn). It is situated on the Nagb Plateau, which forms El Farafra Oasis's northeastern and northern borders. It is not exposed on the study area's surface. Thick fossiliferous lagoonal limestone with an average thickness of 69 meters makes up the majority of the Lower Eocene Farafra Limestone Formation (Tetf), which is exposed at El Quss Abu Said Plateau. Mesozoic (Upper Cretaceous) deposits; Garra Formation; Esna Shale Formation; Tarawan Chalk Formation; Dakhla Formation; Khoman Chalk Formation (Abdel Aziz *et al.,* 1968). It can be found on the slopes of solitary hills and the floor of depressions (Salem *et al.,* 2002).

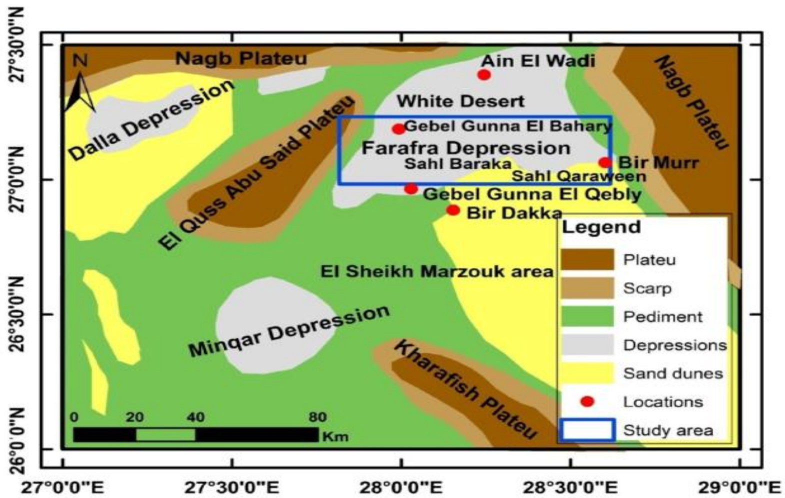

Fig.1: General geomorphic features of El Farafra Depression and its surroundings (after Ali, 2004)

This formation may be as thick as 160 meters below the surface (Barakat *et al.,* 1974). Assessment and prioritization of land for agriculture according to the most important determinants that impede or reduce the productivity of land, as well as in land under rehabilitation, is considered to be arable and relevant. Therefore, land assessment programs have been used in line with the region's climatic conditions, the potential for arable land and its suitability for a number of field crops, fodder and horticulture. Global assessment systems for Mediterranean and dry lands have been used to identify limitations that may hinder or reduce production he collection and analysis of samples, evidence and soil properties can establish a priority map for the commencement of agriculture and then the extent to which these lands are capable of important crops. The current article's goal is to edit a nanocomposite based on Titania and cobalt ferrite for the treatment of contaminated groundwater using iron and manganese ions. The sol gel method was used in the preparation process. Several methods were used to characterize the nanocomposite adsorbent. The adsorption behavior of the adsorbent towards Fe (II) and Mn (II) ions was studied in order to investigate the batch adsorption methodology. Additionally, characterization of the soil involves depth-based investigation. Another scientific study focuses on the interaction between heavy minerals in the soil and water, and crop suitability is advised.

2. Material and Methods

2.1. Sampling techniques

For preparing the standard solutions under a clean laboratory environment analytical chemical grade and deionized water were utilized. Plastic bottles were cleaned through soaking in diluted HNO_3 solution, flushing with deionized water, furthermore drying in an oven the plastic bottles were completely washed with aliquots of the sampled waters, prior to collection. All single standard solutions of different elements were gotten from Merck. Using of calibration standards concentrations of 1g/L (Germany). By using ICPMS (Inductively Coupled Plasma-Mass Spectrometry) the percentage of Recovery for the previously mentioned elements analyzed varied between 90% and 106%. In the field, the samples were gathered from every location in polyethylene bottles. One sample from every location was preserved by acidifying to pH 1.5 with 1 mL of concentrated HNO_3 acid for heavy & trace elements analysis. For field measurements (total dissolved solids (TDS), pH and redox potential (Eh) are mentioned. Techniques for preparing Standard Procedures for Water and Wastewater Examination are mentioned. In order to be analyzed, the samples were transported in a cool box with cooling components to the Central Laboratory for Environmental Quality Monitoring. 32 soil sites from the study area were surveyed as the first step in the current investigation. Thirty-two soil profiles were chosen to represent the selected sites in the area under study. These Ismailia area profiles were excavated to a depth of 150 cm, unless the water table prevented it. It was anticipated that the soil profiles would exhibit significant variances among the farmers. soils, the field book for describing sampling provided the criteria for the morphological description of the soil, which was followed (Pandey *et al.,* 2023). The 32 soil samples that were gathered showed the resulting morphological variations across all soil profile depths. Samples of soil were gathered and prepared for examination in a lab. Particle size distribution was performed using the pipette method for samples with heavy textures, or dry sieving for samples with coarse textures. (Chaudhary *et al.,* 2023). After a measured volume of filtered water was evaporated to dryness at 105 ± 2° C, the solid residue was weighed to determine the total dissolved solids (TDS). After exposing the samples to HCl, the amount of total calcium carbonate was determined, along with the amount of evolved CO_2. (Yadav *et al.,* 2022). Electrical conductivity (EC) and pH values were measured in supernatant and soil water suspensions at a ratio of 1:2.5. The Wet method was used to measure the organic matter. The global positioning system was used to modify the longitudes and latitudes of the water sample locations that were collected (GPS) While some of these parameters (pH and EC) are likely to change while in transit, other parameters, such as depth to water, temperature T°C, and EC, were measured in-situ when gathering water samples (Abdulhady *et al.,* 2021). The measurements were repeated thrice; the calculated range, median and mean were reported. Analytical grade reagents and solvents were used. We bought titanium (IV) isopropoxide (TTIP), ammonium hydroxide (NH_4OH), ferrous chloride tetrahydrate ($FeCl_2.4\ H_2O$), and ferric chloride hexahydrate ($FeCl_3.6\ H_2O$) from Merck. Fe $(NO_3)_2$ or $Mn(NO_3)_2$ salts were used to prepare stock solutions containing 1000 ppm Cu(II) or Pb(II) ions, respectively. Dilution was used to create working metal ion solutions. A plasma-atomic emission spectrometer (ICP-AMS, Optima 3000XL, PerkinElmer) was used to measure the concentrations of metal ions. The Jenway pH meter (model 3310) was used to measure the pH of the solution. During the characterization study, a number of characterization techniques were applied. A spectrophotometer (Perkin Elmer Spectrum Version 10.03.09) was used to obtain FI-IR spectra. Using the Brunauer Emmet, and Teller (BET) on the samples, the surface area, pore size, and pore volume were determined. Using Energy Dispersive Spectroscopy (EDS) and Scanning Electron Microscopy (SEM) Model Quanta 250 FEG (Field Emission Gun), micrographs and analyses of the synthesized nanocomposite were obtained. patterns produced by X-ray diffraction (XRD) using a Schimadzu model X-ray diffractometer. The adsorbent's magnetic properties were assessed using a Vibrating-Sample Magnetometer (VSM, Homade 2 tesla).

2.2. Preparation Technology

2.2.1. Titanium oxide nanoparticles preparation

Sol-gel was used to prepare TiO_2 nanoparticles in accordance with M.H. El-Sayed *et al.,* (2015). In short, distilled water was mixed with titanium (IV) isopropoxide (TTIP), which had been dissolved in absolute ethanol and had a molar ratio of $Ti:H_2O$ = 1:4. Citric acid is used to adjust the pH of the solution to 4.0. Sols were formed by vigorously stirring the solution. Following a 24-hour aging period, the sols were transformed into gel. The gel was then dried for five hours at 100°C to evaporate the water and organic material. Ultimately, sintering the dry at 400°C for 3.0 h produced the required TiO_2 nano-crystalline.

2.2.2. Preparation of Titania coated Co- ferrite nanocomposite

After dissolving the previously prepared TiO_2 in absolute ethanol and distilled water, it was added to a solution containing propylene glycol, $CoSO_4.H_2O$, a molar ratio of (Fe_{3+}/Fe_{2+} = 2), and $FeCl_3.6H_2O$. The pH was adjusted to 4.0 using citric acid. The solution of ammonium hydroxide was added gradually. At 70°C, the solution was agitated vigorously to form the sols and subsequently gel. For five hours, the gel was dried at 100°C. To create the Mn-Nano-Ferrite Titania nanocomposite, the dry gel was sintered at 400°C for 3.0 hours as a last step (Liu *et al.,* 2005).

2.2.3. Land Capability and Suitability Using Applied System of Land Evaluation (ASLE) program

The studied soils were evaluated for land capability and suitability using Applied System of Land Evaluation (ASLE) systems as follow: Qualitative land suitability studies were conducted using Applied System of Land Evaluation (ASLE) program. Other information concerning climatic conditions and agricultural products were also used to Predict the general land capability. From the agriculture point of view, soils of the study area are considered as promising soils. Evaluating their capability is an essential stage for the future practical use. Quantitative estimation of soil characteristics such as slope, drainage conditions (wetness), soil depth, texture, calcium carbonate content, gypsum status, salinity and sodicity were used in the land evaluation. The rating capability and suitability for major crops values and kinds of limitation condition types of the studied soils are:-

Land capability (Index)	Land suitability for crops (Index)
C1 Excellent 80-100	S1 Highly suitable 80-100
C2 Good 60-80	S2 Moderately suitable 60-80
C3 Fair 40-60	S3 Marginally suitable 40-60
C4 Poor 20-40	S4 Conditionally suitable 20-40
C5 Very poor 10-20	NS1 Potentially suitable 10-20
C6 Non-agriculture < 10	NS2 Actually unsuitable < 10

2.2.4. Adsorption methodology

Adsorption study is performed with the aim of discovering the optimal conditions that achieve maximum adsorption for a given adsorbate on a given adsorbent. Batch adsorption methodology is the widely used to evaluate the adsorption percentage as a function of pH, contact time, adsorbent dose, metal ion initial concentration and temperature. The effect of pH on the adsorption process was studied by varying the pH in the range of 1.0– 7.0 by adding either 0.1 M HCl or 0.1 M NaOH. 10 mg adsorbent and metal ion solution (50 mL, 100 mg/L) were mixed in 100 ml flasks and shaken for 60 min. For isotherm studies, 50 mL of varied Cu(II) and Pb(II) ions concentrations, in the range of 50–500 mg/L, was mixed with 10 mg of the adsorbent and shaken as previously mentioned in pH experiments. When the assigned shaking time is over, the TiO_2-Cobalt ferrite nanocomposite was filtered off and the amount Fe(II) and Mn(II) ions was determined by a plasma-atomic emission spectrometer (ICP-AMS, Optima 3000XL, PerkinElmer) in accordance with the Standard Method. The adsorption experiments were carried out triplicate and average values were presented.

$$\text{Adsorption capacity (mg/g)} = [(Co - Ce) / m] \times V$$

Co – Initial conc in ppm, Ce – Conc at equilibrium, (mg L-1), respectively. m – mass of the adsorbent, V is the volume of solution containing solute (adsorbate).

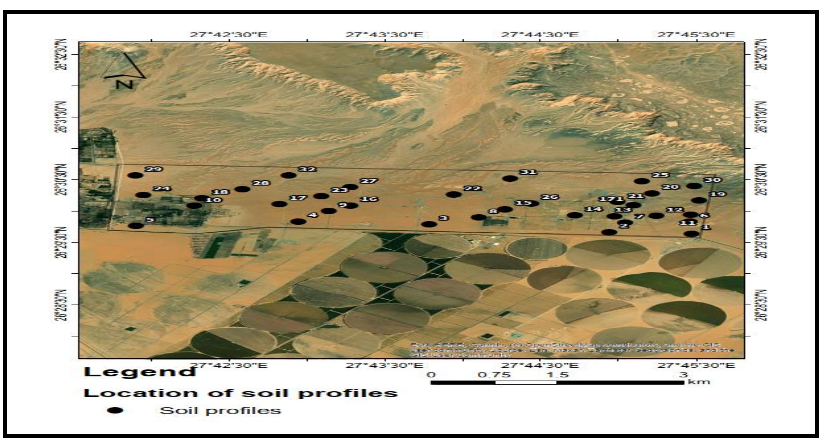

Fig.2: The site map and soil location samples of Abumonkar region (Farafra area)

3. Results and Discussion

3.1. Characterization study of prepared nanocomposite

3.1.1. SEM and EDX analysis

One of the most popular methods for surface analysis is scanning electron microscopy (SEM), which makes it possible to examine the composition and morphology of various structures. In addition, quantitative compositional data and elemental identification are obtained using an Energy Dispersive X-Ray Analyzer (EDX) (Elı'as *et al.,* 2023). The prepared TMFN adsorbent's porosity, which improves adsorption, is reflected in the SEM image with EDX analysis shown in Figure (3 and 4). Furthermore, almost equal-sized large and small particles were seen in the pictures. The presence of titanium (Ti), cobalt (Mn), iron (Fe), and oxygen (O) was verified by EDX measurements, proving that the artificial TiO_2-Cobalt ferrite nanocomposite was successfully formed Table.1. Because of their magnetic characteristics and the binding of the primary particles, which are held together by weak surface interactions like the van der Waals force, the synthesized TiO_2-Cobalt ferrite nanocomposite agglomerated because there was insufficient time for sonication, which results in poor particle separation. Particle agglomeration and irregular morphology, which lack regular shapes, appear to be indicators of the gel formation that occurs when the solution is heated; these characteristics are also seen in the calcined samples.

Table 1: Elemental analysis concentration of synthesized TiO_2-Cobalt ferrite nanocomposite

C	O	Al	S	Cl	Ti	Mn	Fe	Co
4.58	30.31	0.43	1.53	8.15	38.61	0.25	14.18	1.96

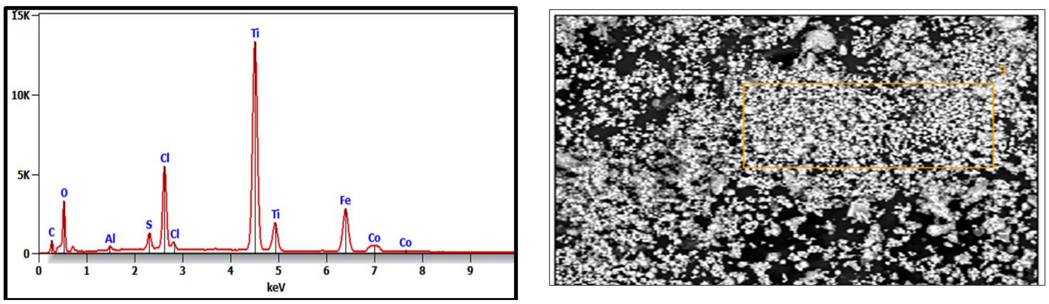

Fig. 3: EDX figure of synthesized TiO_2-Cobalt ferrite nanocomposite

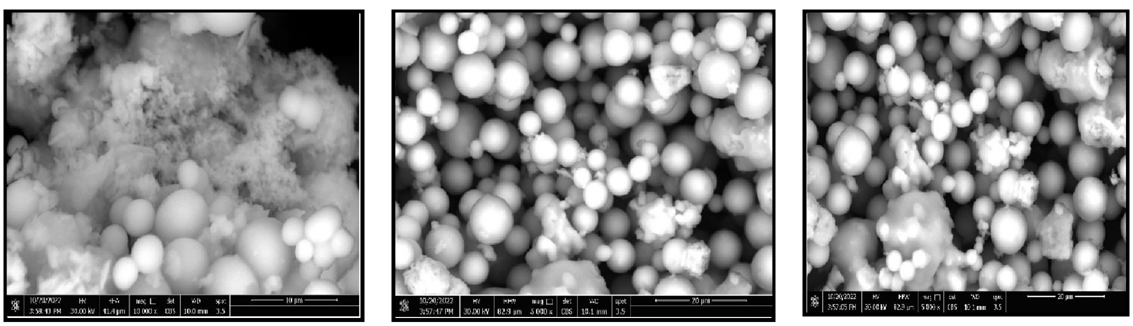

Fig.4: SEM photos of synthesized TiO_2-Cobalt ferrite nanocomposite

3.1.2. FT-IR analysis

When there are unknowns, FT-IR analysis is used to identify the compounds and the general type of material being analyzed. Three main peaks, located at 510 and 620 cm^{-1} below 1000 cm-1 in the FT-IR spectra, are visible for the prepared TiO_2-cobalt ferrite nanocomposite. These are frequently seen in ferrites. The Ti-O bending vibration band was detected at 620 cm-1, whereas the Ti-O-Ti and Ti-O bonds are responsible for the broad band at 500–700 cm^{-1}. The Fe-O bond's bending vibrations are what cause the sharp peaks to form at 510 (Fe_2O_3). The stretching vibration of C-O is responsible for the peak at 1062 cm^{-1}. Conversely, tetrahedral complexes are thought to be responsible for the peak at approximately 500 cm^{-1}. In the FT-IR spectra of each composition, the presence of two typical peaks indicates the formation of the spinel phase in all samples (Sharma *et al.,* 2015). Figure.5

EISSN: 2706-7939 ISSN: 2077-4508 **DOI: 10.36632/ije/2024.13.1.1**

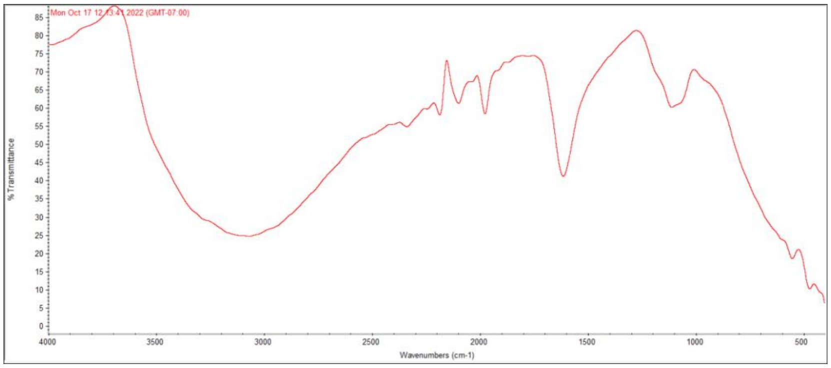

Fig. 5: FT-IR figure of synthesized TiO_2-Cobalt ferrite nanocomposite

3.1.3. Magnetism measurements

Vibrating sample magnetometers (VSMs) were used to characterize a prepared nanocomposite magnetically. The magnetization chart's low hysteresis value indicated that the nanocomposite possessed some paramagnetic strength, which could potentially enhance its ability to attract various pollutants. Materials' magnetic properties are measured using a vibrating sample magnetometer (VSM). Figure.6 displays the magnetization curves for the TiO_2-cobalt ferrite nanocomposite. The prepared nanocomposite exhibits a lower saturation magnetization (Ms) value of 0.512 vs. 23.650 eum/g, in comparison to the pure magnetite nanoparticles. The diamagnetic shell that envelops the magnetite nanoparticles reduces the magnetic moment, which accounts for the observed decrease in saturation magnetizations. Nonetheless, the synthesized TiO_2-Cobalt ferrite nanocomposite exhibits a certain degree of paramagnetic strength, facilitating its separation from.

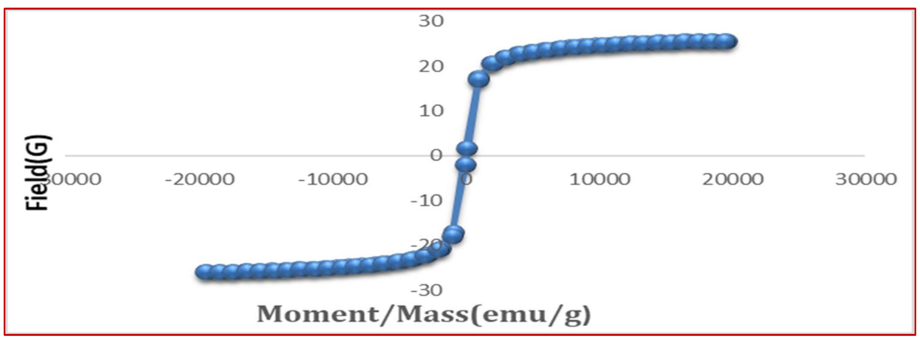

Fig. 6: VSM figure of synthesized TiO_2-Cobalt ferrite nanocomposite

3.1.4. Particle size analysis of synthesized TiO_2-Cobalt ferrite nanocomposite

The synthesized TiO_2-Cobalt ferrite nanocomposites mean particle size and morphology revealed that it has a nearly spherical and crystalline shape. The intensity, volume, and number weightings of the nanoparticles were 58.20 nm, 20.14 nm, and 14.10 nm, respectively Figure.7. The nanocomposite material has a mean diameter of approximately 30.81 nm. This reading indicates that the size, shape, and availability of the dispersion percent in solution are the primary determinants of the reduction percent of the synthesized TiO_2-Cobalt ferrite nanocomposite that is obtained. The main factor influencing the particle size distribution test is an increase in surface area, which increases removal efficiency (Hossain *et al.,* 2018).

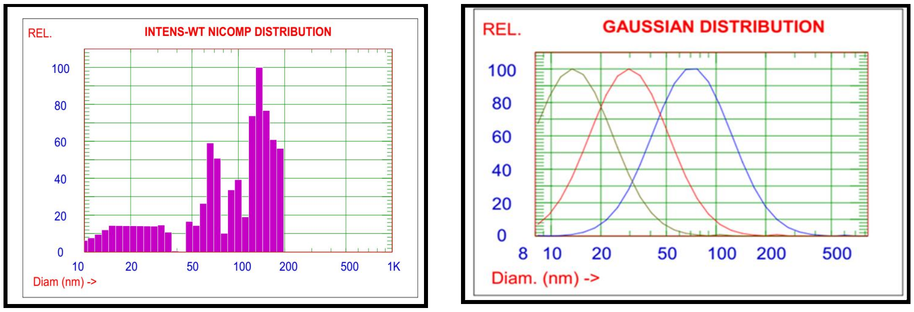

Fig. 7: Particle size distribution of synthesized TiO_2-Cobalt ferrite nanocomposite

3.1.5. XRD analysis

The X-ray diffraction (XRD) patterns of all synthesized samples in the 2θ range of 20–80° are shown in Figure 6. Figure 6 displays the X-ray diffraction (XRD) patterns of all synthesized samples in the 2θ range of 20–80°. An in-depth understanding of a material's chemical makeup, physical characteristics, and crystallographic structure can be obtained through non-destructive X-ray diffraction analysis (XRD). The pattern exhibits five distinct peaks at 2θ, of 22.4°, 32.7°, 34.8°, 40.5° and 48.9°. An in-depth understanding of a material's chemical makeup, physical characteristics, and crystallographic structure can be obtained through non-destructive X-ray diffraction analysis (XRD). The pattern exhibits five distinct peaks at 2θ, which correspond to the diffractions of crystal faces of the Fe_2O_3 and Fe_3O_4 spinal structure. These peaks indicate that the black-colored magnetic powders are a combination of magnetite and hematite nanoparticles (Figure.8). These peaks indicate that the black-colored magnetic powders are a combination of magnetite and hematite nanoparticles. The peaks appeared at 2θ of 25.4° and 39.1° are corresponding to the diffractions of crystal faces of TiO_2 anatase structure. The peak appeared at 2θ of 34.80° is corresponding to the diffractions of crystal faces of coated Cobalt ions on iron oxide nanoparticles (Mahdavi *et al.,* 2007 and Kefeni *et al.,* 2017).

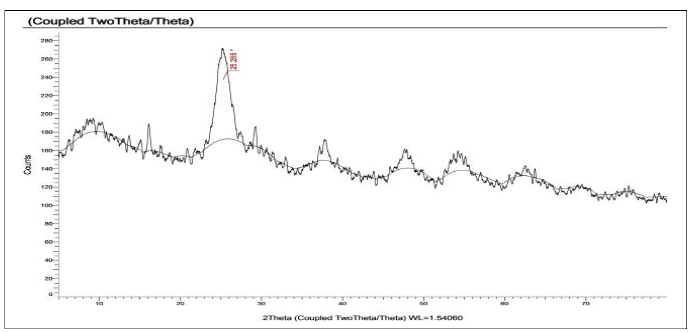

Fig. 8: XRD chart of synthesized TiO_2-Cobalt ferrite nanocomposite

3.1.6. Nitrogen adsorption-desorption isotherm

A well-established and popular method for figuring out a compound's specific surface area and pore size distribution is nitrogen adsorption at low temperatures. Synthesized TiO_2-Cobalt ferrite nanocomposite pore-size distribution curve and nitrogen adsorption-desorption isotherm. The typical hysteresis loops of mesoporous materials are displayed by the TiO_2-Cobalt ferrite nanocomposite. It was discovered that the pore diameter, pore volume, and specific surface area were, respectively, 14.21 nm, 0.0107 cc/g, and 3.06 m^2/g (Gherca *et al.,* 2010).

3.1.7. Investigation of BET/adsorption charts of synthesized TiO_2-Cobalt ferrite nanocomposite

The powder's BET was discovered to have a median pore diameter of 32.14 and an average pore diameter of 5.20. The majority of the nanocomposite was smaller than 20 nm. The newly formed chemical structure is to blame for this. The production of new nanostructures connected to the iron nano core by multiple hydroxyl groups was largely facilitated by the inorganic salts of manganese, copper, and zinc. The multilayer covering the new third layer can continue the adsorption process. At low adsorption densities, the Langmuir adsorption isotherms predict linear adsorption; at higher solute metal concentrations, they predict maximum surface coverage. For monolayer adsorption onto a homogeneous surface, Langmuir adsorption is essential. When adsorbed species do not interact with one another (Langmuir, 1918) (Figure.9). T-Plot / This method require a "thickness function," which expresses the thickness of adsorbate layers on a non-porous surface as a function of pressure, in addition to an isotherm. The t-plot approach makes an effort to connect the adsorption on a substance with a model curve that indicates the surface thickness of the adsorbed layer. The thickness values derived from the model are plotted against the isotherm loading data in a constructed plot. The model-fitted experimental adsorption curve yields a straight line whose intercept passes through the origin. Condensation in a certain kind of pore will be indicated by a sharp vertical deviation. Adsorption on a specific pore wall will be indicated by a gradual slope. The area must be calculated in order to determine the line section's slope. The material's entire surface area will be depicted. The line's intercept won't go through the origin anymore. The T-plot technique observed the variations between an ideal adsorption curve and the isotherm. Consideration of the material and adsorbate is crucial when selecting a thickness model. There is no physical significance to interference that appears on the t-plot below the thickness of the monolayer (Lippens *et al.,* (1965). Furthermore, the MP method is the most effective method for adsorbents when the micro pore analysis is completed. Hassan MR *et al.,* (2021).

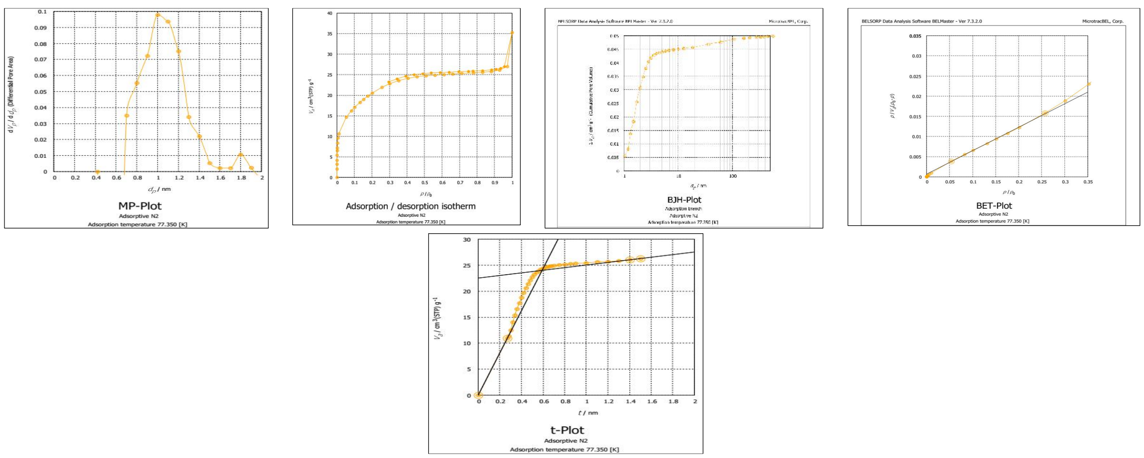

Fig. 9: BET spectrum of synthesized TiO_2-Cobalt ferrite nanocomposite

3.2. Chemical analyses of major cations & anions of groundwater of in the Dakhla-Abu Minqar District

According to a chemical analysis, fresh water can have a salinity value within a certain range (Table 2). The concentration of total suspended substances (TSS) was within an acceptable range for agricultural use.

Table 2: Chemical analyses of major cations & anions of groundwater of in the Dakhla-Abu Minqar District

ID	pH	EC µs/cm	TDS ppm	Soluble Cations ppm				Soluble Anions ppm			
				K^+	Na^+	Mg^{++}	Ca^{++}	Cl^-	SO_4^{--}	HCO_3^-	CO_3^{--}
GR1	8.01	773	495	13	80	24	58	190	70	117	0.78
GR2	7.88	655	419	12	65	22	50	146	62	126	0.54
GR3	7.90	860	550	15	100	29	68	205	74	119	1.05
Mean	**7.9**	**762.7**	**488.0**	**13.3**	**81.7**	**25.0**	**58.7**	**180.3**	**68.7**	**120.7**	**1.67**
Minimum	7.90	655	419	12	65	22	50	146	62	117	0.54
Maximum	8.01	860	550	15	100	29	68	205	74	119	1.05

Table 3: Chemical and biological analyses of groundwater samples of in the Dakhla-Abu Minqar District

ID	pH	EC µs/cm	TDS $Mg.L^{-1}$	TSS $Mg.L^{-1}$	COD $Mg.L^{-1}$	BOD $Mg.L^{-1}$	TN $Mg.L^{-1}$	TP $Mg.L^{-1}$
GR1	8.01	773	495	3.20	6.50	2.20	1.80	0.15
GR2	7.88	655	419	2.89	8.40	1.90	2.87	0.20
GR3	7.90	860	550	4.01	7.02	1.57	2.69	0.26
Mean	7.9	762	488	3.4	7.3	1.89	2.5	0.2
Minimum	7.90	655	419	2.89	6.50	1.57	1.80	0.15
Maximum	8.01	860	550	4.01	8.40	2.20	2.87	0.26

WS: water surface; WG: Ground Water; COD: Chemical oxygen demand; BOD: Biological oxygen demand; TSS: Total suspended solids

The primary analysis that had an impact on the quality of groundwater revealed that bed rock dissolution and interaction with rainfall had contaminated the area. The average chemical oxygen dissolved (COD) was 7.30 ppm, which is within the acceptable range for effective irrigation in agriculture. The water's BOD (biochemical oxygen dissolved) value was 1.89 parts per million in this instance, which is below the recommended level for microbial pollution. The concentrations of total phosphorus (TP) and total nitrogen (TP) were within allowable bounds. The concentration of total suspended substance (TSS) was within a permissible limit for agriculture, ranging from 2.89 to 4.01 ppm.

3.3. Chemical analyses of heavy metals of groundwater of in the Dakhla-Abu Minqar District

The heavy metals content in all samples of groundwater in a limited standard ranges except for iron and manganese ions. The main problem in irrigation process in target area is the raising of Fe & Mn concentrations in groundwater that has a bad effect on crop productivity and ecosystem environment (Braul *et al.,* 1998) Table.4. Iron in groundwater quickly oxidizes to a reddish-brown product (hydrated iron oxide) when exposed to air. Iron is a common water contaminant that is not considered a health hazard; however, its presence at elevated levels can cause aesthetic problems on ornamental plants, buildings and structures, and its accumulation on irrigation equipment can lead to clogged emitters. Iron can be present in a water supply in many different forms (soluble, chelated, organic, and precipitated) and may or may not be apparent to the eye. These forms include ferrous (Fe^{+2}) or dissolved iron, which is invisible, while the ferric (Fe^{+3}) or oxidized (rusted) iron becomes apparent through precipitation, and usually appears as brownish red colored particles suspended in the water (Braul *et al.,* 1989). Irrigation water with iron levels above 0.1 ppm may cause clogging of drip irrigation emitters and above 0.3 ppm may lead to iron rust stains, and discoloration on foliage plants in overhead irrigation applications. These levels are generally below the levels that cause toxicities in plant tissue except when iron levels exceed 4 ppm or when the root medium pH is below 5.5. (Clark *et al.,* 2002; Nakayama *et al.,* 2005).

Table 4: Chemical analyses of heavy metals of groundwater of in the Dakhla-Abu Minqar District

ID	Al	Cd	Co	Cr	Cu	Fe	Mn	Mo	Ni	Pb	V	Zn
	ppm											
GR1	0.03	0.05	0.06	0.01	0.13	6.70	1.56	ND	ND	0.32	ND	0.02
GR2	0.05	0.02	0.08	0.03	0.15	11.50	0.97	ND	ND	0.54	ND	0.04
GR3	0.06	0.04	0.04	0.02	0.18	8.90	1.20	ND	ND	0.17	ND	0.01
Mean	0.05	0.04	0.06	0.02	0.15	9.03	1.24	ND	ND	0.34	ND	0.02
Minimum	0.03	0.02	0.04	0.01	0.13	6.70	0.97	ND	ND	0.17	ND	0.01
Maximum	0.06	0.05	0.08	0.03	0.18	11.50	1.56	ND	ND	0.54	ND	0.04

3.4. Optimal conditions of synthesized TiO_2-Cobalt ferrite nanocomposite for removal polluted iron and manganese ions

Table 5. Showed the different parameters such as pH & contact time & temperature and dosing of synthesized TiO_2-Cobalt ferrite nanocomposite on removal of polluted heavy metals. For iron removal the best optimal conditions is nanocomposite dosage: 0.3 g/l; Contact time: 20 min.; Temp.:

45ºC; PH: 6.0. Also, for Mn removal the best optimal conditions is Optimal conditions; nanocomposite dosage: 0.3 g/l; Contact time: 20 min.; Temp.: 45oC; PH: 5.0.

Table 5: Optimal conditions of synthesized TiO_2-Cobalt ferrite nanocomposite for removal iron metal

pH	Nanocomposite Dose (g/l)	Removal %	Contact Time	Nanocomposite Dose (g/l)	Removal %
4	0.3 g/l	78.20	10	0.3 g/l	78.30
5		88.14	20		91.22
6		90.54	30		89.00
8		85.98	40		86.98
Temp. ºC	**Nanocomposite Dose (g/l)**	**Removal %**	**Nanocomposite Dose (g/l)**	**Removal %**	
25	0.3 g/l	86.00	0.1	60.05	
35		87.52	0.2	94.86	
45		92.57	0.3	95.98	
60		85.31	0.4	95.21	

Optimal conditions; Nanocomposite dosage: 0.3 g/l; Contact time: 20 min.; Temp.: 45ºC; PH: 6.0

Table 6: Optimal conditions of synthesized TiO_2-Cobalt ferrite nanocomposite for removal manganese metal

pH	Nanocomposite Dose (g/l)	Removal %	Contact time	Nanocomposite Dose (g/l)	Removal (%)
4	0.3 g/l	88.60	10	0.3 g/l	84.00
5		91.25	20		89.14
6		89.57	30		88.63
8		86.04	40		86.79
Temp. ºC	**Nanocomposite Dose (g/l)**	**Removal %**	**Nanocomposite Dose (g/l)**	**Removal %**	
25	0.3 g/l	86.00	0.1	55.00	
35		87.52	0.2	90.74	
45		92.57	0.3	91.74	
60		85.31	0.4	91.00	

Optimal conditions; Nanocomposite dosage: 0.3 g/l; Contact time: 20 min.; Temp.: 45ºC; PH: 5.0

Removal percent of iron and manganese ions from polluted groundwater

Table 7. showed the positive removal effect of synthesized TiO_2-Cobalt ferrite nanocomposite on polluted iron and manganese ions (groundwater). The mean value of iron removal % is 92.73% at Optimal conditions; Nanocomposite dosage: 0.3 g/l; Contact time: 20 min.; Temp.: 45oC; PH: 6.0. Also, the mean value of manganese removal % is 82.91% at Optimal conditions; Nanocomposite dosage: 0.3 g/l; Contact time: 20 min.; Temp.: 45ºC; PH: 5.0.

Table 7: Removal percent of iron and manganese ions from polluted groundwater

Parameter mg/l	Permissible limit (USSL)	Before treatment	After treatment	Removal (%)	Adsorption Capacity (mg/g)
Iron	<0.3	6.70	0.35	94.70	174.66
	<0.3	11.50	1.02	91.10	
	<0.3	8.90	0.67	92.40	
		Mean		92.73	
Optimal conditions; Nanocomposite dosage: 0.3 g/l; Contact time: 20 min.; Temp.: 45ºC; pH: 6.0					
Manganese	<0.2	1.56	0.21	86.50	156.16
	<0.2	0.97	0.18	81.44	
	<0.2	1.20	0.23	80.80	
		Mean		82.91	

Optimal conditions; Nanocomposite dosage: 0.3 g/l ; Contact time: 20 min.; Temp.: 45ºC; pH: 5.0

Adsorption results

Adsorption mechanism

The pH of the working solution has a significant impact on the mechanism of metal ion adsorption on a particular adsorbent. The adsorbent's surface chemistry and the solution chemistry of the adsorbed metal ions are both influenced by the pH of the solution (Miyah *et al.,* 2017). Due to the electrostatic repulsion between the positive surface of the adsorbent and the positive metal ions, the adsorption of Fe (II) and Mn (II) ions on the prepared adsorbent is not preferred at low pH values. More metal ions are adsorbed and the adsorbent's surface becomes more negative as pH rises. At pH between 5.0 to 6.0, the maximum adsorption percentage was found. This is because the surface of the adsorbent is quite negatively charged and attracts more of the positively charged metal ions. This occurs as a result of the adsorbent's highly negatively charged surface drawing in more positively charged metal ions.

The role importance of pH

The pH affects a nanomaterial's surface characteristics. Because of the deprotonating of functional groups, the surface of nanomaterials generally has a positive charge at low pH values and a more negative charge as pH rises. Furthermore, the Fe (II) and Mn (II) ions chemistry is influenced by the pH of the solution (Kumar *et al.,* 2014). Iron and manganese ions, or Fe (II) and Mn (II) ions, are primarily present as free positively charged ions at pH values lower than 5.0. Iron and manganese ions precipitate as hydroxides above pH 5.0, or they can even form positively charged soluble complexes (Kumar *et al.,* 2019).

The adsorption % of Mn (II) and Fe (II) ions is low at low pH values. The decrease in adsorption percentage can be attributed to the positively charged nature of metal ions and the adsorbent surface, as well as the electrostatic repulsion between the protonated surface of the synthesized TiO_2-Cobalt ferrite nanocomposite surface and the positive metal ions present in the medium. Because the adsorbent surface becomes more negative as pH rises, the adsorption percentage for both Mn (II) and Fe (II) ions begins to rise. At pH 5.0, the maximum adsorption percentages for Mn (II) were 91% and 90% for Fe (II) at pH 6. The adsorption percentages decrease above pH 6.0.

Adsorbent dosage dependence

We looked at four different doses of the adsorbent—0.1, 0.2, 0.3, and 0.4 g/L to see how they affected the adsorption percentage. The findings demonstrated a direct relationship between the amount of adsorbent in the solution and the adsorption percentage. The removal percentages for Fe (II) and Mn (II) increased from 55 to 90.74% and from 60.05 to 94.86%, respectively, when the dosage was increased from 0.1 to 0.2 g/L. This observation is explained by the fact that adding more adsorbent to the solution increases the number of active sites. Because there are less metal ions in relation to the amount of adsorbent, a further increase in dosage has a slight impact on the removal percentages. (Mahmoodi *et al.,* 2018) Table.8.

Table 8: The removal % of Fe (II) & Mn (II) ions VS Nanocomposite dose

Fe (II) ions		**Mn (II) ions**	
Nanocomposite Dose (g/L)	**Removal %**	**Nanocomposite Dose (g/L)**	**Removal %**
0.1	60.05	0.1	55.00
0.2	94.86	0.2	90.74
0.3	95.98	0.3	91.74
0.4	95.21	0.4	91.00

Adsorbent regeneration and reuse

From an economic perspective, adsorbent regeneration and reuse are crucial. Adsorbents with a high adsorption capacity and that are reusable are strongly advised. In this work, the regeneration step was carried out by filtering and shaking the adsorbent for 1.0 hours at 25°C using 20 mL of 0.1 M HCl following each adsorption cycle. Following that, the regenerate adsorbent was dried at 80°C, filtered, and cleaned with distilled water before being used again to adsorb Fe (II) and Mn (II) ions. Even after eight consecutive adsorption-desorption cycles, the synthesized TiO2-Cobalt ferrite nanocomposite was still able to remove up to 60% and 57% of Fe (II) and Mn (II) ions from polluted groundwater, respectively, as shown in Table.9

Table 9: Adsorbent reusability of synthesized TiO_2-Cobalt ferrite nanocomposite

	Reusability cycles/Removal efficiency (%)							
Pollutants	**1**	**2**	**3**	**4**	**5**	**6**	**7**	**8**
Fe (II)	90	85	80	72	70	65	62	60
Mn (II)	88	84	79	71	68	65	60	57

The relationship between subsurface depth & soil properties and physical texture

The entire soil analysis, which included a sieving analysis, revealed the variations in soil texture between the sites. The target area's eastern and western locations have different percentages of particle size distribution in their soil samples. It has low levels of gravel and a range of fine to coarse sand particles, depending on the sieving analysis. The silty clay minerals intercalated with increasing soil particle size from the surface to the subsurface. Subsurface samples show varying soil types in the soil profile with depth. We discovered that the subsurface soil had a distinct texture, ranging from coarse and sandy to silt and clay intercalated Table.10. Certain soil profiles had subsurface intercalated clay with varying mineralization contents and high surface sector carbonate content. Furthermore, the dissolution and leaching process of silty clay minerals and alkali or earthy minerals may be the cause of high sodium content in the subsurface as opposed to the surface. This could be brought on by the clay content of the soil, which acts as an insulating layer. Table. The inability to continue digging below the surface was demonstrated in profiles 6, 7, 9, 10, 12, 13, 16, 18, 21, 23, 27, 28, 29, and 30. This is because the hardness layers intercalated with one another, negatively affecting the agriculture of various crops.

Table 10: Relationship between soil depth and Particle size distribution (%)

P No	**Depth / Cm**	**Texture**	**Particle size distribution (%)**					**Sand**	**Silt**	**Clay**
			2-1	**1-0.5**	**0.5-0.25**	**0.25-0.125**	**0.125-0.063**			
1	0-30	S	0.50	17.50	79.50	2.00	0.50	-	-	-
	30-90	SL	-	-	-	-	-	75.15	6.70	18.15
	90-120	SL	-	-	-	-	-	62.15	24.70	13.15
2	0-50	S	1.50	21.50	60.50	12.50	3.00	1.00	-	-
	50-100	SL	-	-	-	-	-	65.00	20.00	15.00
	100-130	Sl	-	-	-	-	-	65.00	20.00	15.00
3	0-50	S	5.00	21.50	57.50	8.00	3.50	4.50	-	-
	50-110	Sl	-	-	-	-	-	65.00	15.00	20.00
4	0-55	S	1.08	13.66	32.24	34.24	17.60	1.18		
	55-110	SL	-	-	-	-	-	64.15	20.70	15.15
	110-130	SL	-	-	-	-	-	66.25	21.60	12.15
5	0--50	s	6.90	10.50	33.21	34.07	13.15	2.17		
	50-100	SCL	-	-	-	-	-	55.15	12.75	32.10
6	0-25	S	8.59	4.04	24.49	38.21	20.33	4.34		
	25-50	CL	-	-	-	-	-	32.00	33.00	35.00
7	0-30	SL	-	-	-	-	-	65.00	20.00	15.00
	30-60	SL	-	-	-	-	-	65.00	15.00	20.00
8	0-40	S	11.25	7.53	24.23	30.93	21.02	5.04		
	40-80	Sl	-	-	-	-	-	65.00	15.00	20.00
	80-120	SCL	-	-	-	-	-	52.02	14.98	33.00
9	0-35	SL	-	-	-	-	-	62.15	24.70	13.15
10	0-45	SL	-	-	-	-	-	62.15	24.70	13.15
11	0--50	s	2.33	6.50	34.16	39.73	16.04	1.24		
	50-100	s	6.66	2.02	18.36	42.74	26.11	4.11		
	100-120	sL	-	-	-	-	-	65.00	20.00	15.00
12	0--35	sl	-	-	-	-	-	62.15	24.70	13.15
13	0-30	sL	-	-	-	-	-	65.00	20.00	15.00
14	0-50	MS	8.00	61.00	21.50	5.50	2.50	1.50	-	-
	50-100	MS	1.50	37.50	46.00	5.00	5.00	2.00	-	-
	100-150	LS								
15	0-50	SL	-	-	-	-	-	65.00	15.00	20.00
	50-100	SCL	-	-	-	-	-	55.00	12.86	32.14
16	0-30	SCL	-	-	-	-	-	55.12	15.73	29.15

17	0-20	CL	-	-	-	-	-	42.20	30.00	27.80
	0-25	SL	-	-	-	-	-	65.00	15.00	20.00
	25-75	SCL	-	-	-	-	-	55.12	15.73	29.15
	75-130	CL	-	-	-	-	-	32.15	33.85	34.00
18	0-35	sL	-	-	-	-	-	65.00	20.00	15.00
19	0--25	Sl	-	-	-	-	-	65.00	15.00	20.00
	25-45	Cl	-	-	-	-	-	32.00	33.00	35.00
20	0-30	S	14.50	61.00	16.50	6.50	1.00	0.50	-	-
	30-60	Sl	-	-	-	-	-	65.00	20.00	15.00
	60-90	SCL	-	-	-	-	-	60.00	8.00	32.00
21	0-25	SCL	-	-	-	-	-	60.00	8.00	32.00
	25-55	SCL	-	-	-	-	-	59.00	7.00	34.00
22	0-35	LS	-	-	-	-	-	75.00	15.00	10.00
	35-90	SCL	-	-	-	-	-	60.00	8.00	32.00
23	0-30	SL	-	-	-	-	-	65.00	20.00	15.00
	30-60	SL	-	-	-	-	-	65.00	15.00	20.00
24	0-35	SL	-	-	-	-	-	65.00	20.00	15.00
	35-85	SCL	-	-	-	-	-	55.15	12.75	32.10
25	0-30	SL	-	-	-	-	-	65.00	20.00	15.00
	30-80	SL	-	-	-	-	-	65.00	15.00	20.00
	80-150	SCL	-	-	-	-	-	52.02	14.98	33.00
26	0-30	SL	-	-	-	-	-	65.00	15.00	20.00
	30-100	SL	-	-	-	-	-	62.15	24.70	13.15
	100-150	CL	-	-	-	-	-	29.00	32.70	36.30
27	0-60	SL	-	-	-	-	-	62.15	24.70	13.15
28	0-35	SL	-	-	-	-	-	65.00	15.00	20.00
29	0-40	C	-	-	-	-	-	20.15	39.37	40.48
30	0-25	C	-	-	-	-	-	23.15	22.73	54.12
31	0-20	SL	-	-	-	-	-	62.15	24.70	13.15
32	0-45	MS	1.50	44.50	35.00	10.00	6.50	2.50	-	-
	45-90	CL	-	-	-	-	-	30.15	32.70	37.15

Relationship between soil depth and major ionic content

Table 11. Explained the cationic and anionic content of soil with subsurface layers. Also, the analytical results of soil salinity showed the big difference from surface to subsurface with depth. The raising of salinity values may be due to the increasing of precipitation minerals with increase ionic intercalation.

Table 11: Relationship between soil depth and soluble cation and anions concentration

P No.	EC dS /m	Cationic Anions				Anionic Anions			
		Ca^{++}	Mg^{++}	K^{+}	Na^{+}	Cl^{-}	HCO_3^{-}	CO_3^{--}	SO_4^{--}
		Mg/L^{-1}							
1	3.08	14.1	6.88	0.77	32.73	10.57	6.5	-	37.41
	15.71	35.94	17.97	6.88	126.65	107.25	3	-	77.19
	15.13	35.19	17.22	6.13	125.9	106.5	2.25		76.44
2	2.89	13.32	2.78	1.23	11.86	5.76	2	-	21.44
	14.2	29.6	13.73	6.85	138.21	158.62	4.5	-	25.28
	13.4	5.89	2.62	2.78	52.32	47	3	-	13.6
3	3.12	13.48	2.72	1.22	14.89	7.84	3	-	21.46
	14.4	4.85	1.13	0.96	73.46	62	3	-	15.4
4	3.91	17.86	7.06	2.66	11.63	1.65	2	-	35.56
	23	55.46	25.32	8.41	202.41	240.87	2.5	-	48.23
	24.1	60.49	32.12	8.17	216.02	263.37	2.5	-	50.93
5	2.6	4.12	1.82	0.38	103.6	56.6	3.5	-	48.82
	13.2	4.46	1.4	0.63	99.83	7.76	2.5	-	96.07
6	3.41	28.6	11.11	1.55	81.6	68.9	2.6	-	51.3
	12.35	119.44	60.53	4.85	10.66	13.50	2.00	-	179.98
7	4.19	27.83	12.6	0.57	63.16	28.75	4.5	-	43.91
	6.63	16.08	4.97	5.67	4.97	10	1	-	19.7
8	3.6	4.12	1.82	0.38	103.6	56.6	3.5	-	48.82
	13.2	37.59	7.16	13.25	139.64	4.32	2.5	-	190.82
	8.2	28.57	13.44	1.76	63.02	39.50	1.50	-	65.80
9	4.6	0.20	0.06	0.03	1.41	1.12	0.50	-	0.08
10	8.07	32.66	14.84	1.01	83.13	88.12	2.00	-	41.52

	3.2	3.36	0.64	0.7	28.3	9.6	5	-	18.4
11	4.1	0.20	0.06	0.03	1.41	1.12	0.50	-	0.08
	7.6	9.15	3.12	1.37	78.16	20.16	1.00	-	70.64
12	5.7	21.31	5.02	3.77	31.10	13.00	2.00	-	46.20
13	4.8	0.20	0.06	0.03	1.41	1.12	0.50	-	0.08
	2.68	60.63	20.26	6.47	458.64	538	3	-	5
14	3.55	19.97	5.8	3.48	76	6.13	5	-	94.12
	3.17	15.28	5.22	1.04	11.26	1.41	1.50	-	29.89
15	3.28	3.36	0.64	0.70	28.30	9.60	5.00	-	18.40
	21.3	62.26	37.36	5.81	252.2	331	5.5	-	21.1
16	8.9	28.57	13.44	1.76	63.02	39.50	1.50	-	65.80
17	10.2	33.21	14.76	1.37	81.23	70.50	1.00	-	59.06
17	5.7	21.31	5.02	3.77	31.10	13.00	2.00	-	46.20
	12.6	119.44	60.53	4.85	10.66	13.50	2.00	-	179.98
	14.8	41.20	19.28	3.95	167.16	193.87	1.00	-	36.73
18	10.2	33.21	14.76	1.37	81.23	70.5	1	-	59.06
19	4.3	0.20	0.06	0.03	1.41	1.12	0.50	-	0.08
	8.9	28.35	8.13	3.85	14.87	4.8	3	-	47.4
	2.4	11.15	4.92	2.23	9.51	1.41	1.50	-	24.89
20	5.8	26.90	14.33	1.98	59.98	28.20	2.50	-	72.50
	15.2	35.94	17.97	6.88	126.65	107.25	3	-	77.19
21	4.89	21.31	5.02	3.77	31.1	13	2	-	46.2
	23.4	60.49	32.12	8.17	216.02	263.37	2.5	-	50.93
22	16.52	61.33	29.47	6.26	238.94	305.5	3.5	-	27
	36.2	85.2	25.35	18.02	596.2	700	3.5	-	21.3
23	3.71	66.88	22.29	32.99	26.3	28.3	1.5	-	38.3
	7.31	28.57	13.44	1.76	63.02	39.5	1.5	-	65.8
24	4.2	0.01	0.01	0.01	24.37	21.15	1.5	-	1.75
	7.8	28.57	13.44	1.76	63.02	39.50	1.50	-	65.80
	3.98	6.12	2.8	3.55	22.53	15.12	1.5	-	18.38
25	8.72	11.25	3.81	3.36	6.58	1.88	1.5	-	21.62
	6.4	26.90	14.33	1.98	59.98	28.20	2.50	-	72.50
	2.11	10.89	5.53	1.82	63.72	19.92	4.00	-	58.04
26	7.35	28.57	13.44	1.76	63.02	39.50	1.50	-	65.80
	6.63	26.90	14.33	1.98	59.98	28.20	2.50	-	72.50
27	9.12	32.66	14.84	1.01	83.13	88.12	2.00	-	41.52
28	3.16	23.31	10.53	1.58	47.75	31.2	1.5	-	50.46
29	50.8	62.69	21.34	24.48	957.09	1008	5	-	52.6
30	32.6	62.69	21.34	24.48	957.09	1008	5	-	52.6
31	14.2	119.44	60.53	4.85	10.66	13.50	2.00	-	179.98
32	4.58	17.89	6.04	1.26	44.42	60.96	2.00	-	6.64
	39.8	96.36	33.79	12.11	362.93	283.2	5	-	217

The relationship of physical features with soil depth and salinity of in the Dakhla-Abu Minqar District

The $CaCO_3$ content in the majority of site samples was within standard ranges, meaning there was little risk to agricultural productivity. Every land has low levels of organic matter and nutrients, and in order to increase strength, construction, and fertility, a significant amount of organic matter must be added. In certain cases, rare nutrient levels are low, and in others, weak. Despite the area's geological makeup, especially in lowlands in the north with a proportion of mud and girl child, the plant may not benefit from the high soil reaction number (pH). Instead, it is preferable to add organic matter, agricultural plaster, and good management to overcome salinity issues and to take advantage of nutrients. Due to the poor qualities of some soils, particularly those that is shallow, very shallow, and highly salted.

Soil depth

Soil depth is the main factor in the use and cultivation of soil and then salinity, texture and drainage. As a result of the different depth of the soil, it can be divided into deep segments of more than 100 to 125 centimeters or 125 to 150 centimeters. It is located in the first land on the side of the road (oases inside - Farafra). Medium-depth sectors are usually between semi-level and low-sand areas, especially in the middle of the area (50-100 cm). Shallow segments (50-25 cm) then very shallow less than 25 cm. The bottom of the soil is usually a salty child or rock. Figure.10

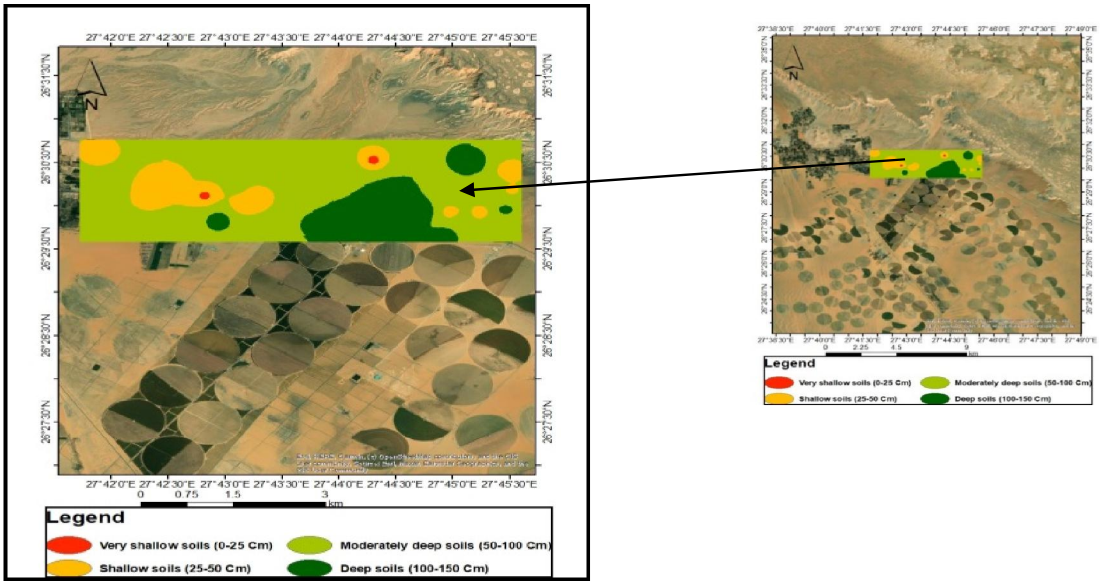

Fig. 10: Distribution maps of soil depth on in the Dakhla-Abu Minqar District

Soil Salinity

Crop cultivation and productivity are determined by salinity, which comes after depth. In the next years, soil salinity is predicted to have a more significant and global impact. Water resources' salinity is correlated with increasing land salinization. According to Cetin and Kirda (2003), soil irrigation directly correlates with a decrease in soil salinity. The most detrimental element affecting plant growth is the salinity of the soil. Productivity decreases by more than 10% as salinity rises by 1-3 millimeters/cm. The majority of the soil extract samples from this farm have varied salinities, but they are primarily high salinities, according to the findings of the electrical conductivity study. which reaches very, very high salinity. Salinity with depth and strength are important determinants of agriculture priorities, and in this region salinity is the most important factor due to the use of modern irrigation. The electrical conductivity (EC) values of the soil's water extract range from less than 2 to 50 millimeters/m with a general trend of increase with depth. The cationic composition of soil extract is dominated by sodium followed by calcium, magnesium and potassium. In most cases, anionic composition follows the order of the following sulfate greater than chloride, and in a few cases, the concentration of chloride ion is higher than sulfate. Thus, the prevailing salts are predominantly sulfate and sodium chloride, calcium chloride, sodium and sodium bicarbonate. In shallow lands, which are already the highest saline areas, care must be taken and salts must be disposed of, whether drains or washing in the form of terraces and basins. The soil laundry needs of each region are calculated and the liquid needs are added before planting of each crop but preferably before planting and after adding organic matter. Especially in the new valley, must adhere to continuous irrigation operations to keep salts away from root proliferation areas. The importance of assessing the soil's interaction is due to its direct impact on the degree of viability and the extent to which the nutrients available in the soil can absorb the plant. The soil thus exhibited a moderate to highly alkaline-affected reaction, with the pH value of the studied samples ranging from 7.8 to 8.7. Since these lands are land intended for cultivation, organic matter must be added and mixed with soil to make the elements more accessible. The average soil alkalinity within the soil sector is from 7.8 to 8.4 Figure.11.

Int. J. Envi., 13(1): 1-26, 2024
EISSN: 2706-7939 ISSN: 2077-4508 **DOI: 10.36632/ije/2024.13.1.1**

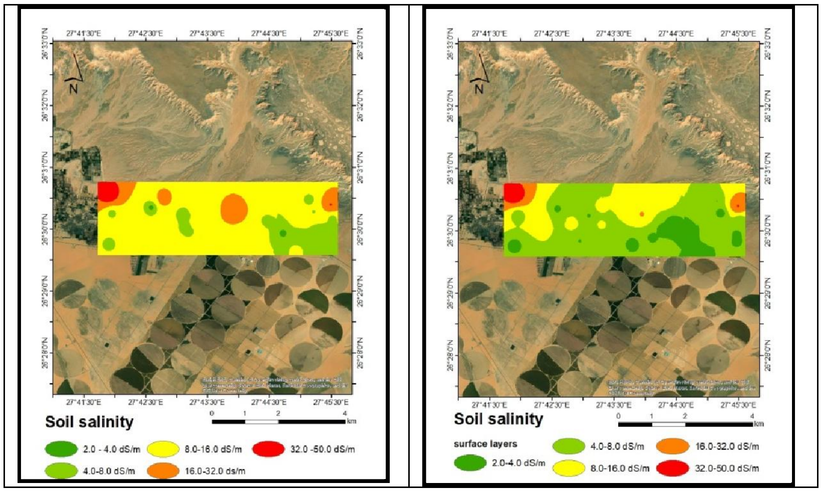

Fig. 11: Distribution maps of soil salinity on in the Dakhla-Abu Minqar District

Land Capability Classification

Evaluation of land capability and suitability was carried out using ASLE (The Applied System of Land Evaluation) software according to Ismail and Morsi (2001). Most of the land characteristics that were considered in the evaluation of the current land units under irrigation, ranged from very favorable to favorable for agricultural purposes. Qualitative land suitability studies were conducted using Applied System of Land Evaluation (ASLE) program. Other information concerning climatic conditions and agricultural products were also used to predict the general land capability. From the agriculture point of view, soils of the study area are considered as promising soils. Evaluating their capability is an essential stage for the future practical use (Figure.13). Quantitative estimation of soil characteristics such as slope, drainage conditions (wetness), soil depth, texture, calcium carbonate content, gypsum status, salinity and sodicity were used in the land evaluation. The rating capability values and kinds of limitation condition types of the studied soils. Accordingly, the study area could be classified into three classes as follow; Class 3 (Fair): This class contains the soils which have marginally suitable capability class C3 (ASLE program), The soils of this class are affected by moderate limitations Class 4 (Poor): According to ASLE program this class comprises the soils which are not suitable for agricultural use, but they are suitable for pasture, have severe limitations that can be corrected and cover 45% of the study area. It could be concluded that the applied system of land evaluation (ASLE) is the most suitable program. It is preferable to be used as a qualitative land capability system for agricultural purposes. ASLE program can be also used by decision makers when they plan for future land utilization. The results of the current study indicated that the most limiting factors were soil texture followed by soil depth and soil salinity. Very poor soils (C5): The soils of this class have very severe limitations mainly of shallow and very shallow soils. These soils require very careful management and special conservation (Figure.12 and Table.12).

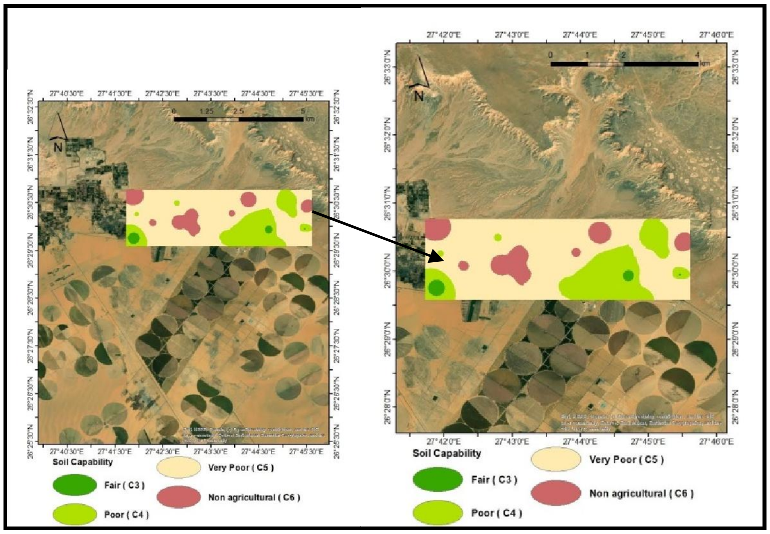

Fig. 12: Distribution maps of land capability on in the Dakhla-Abu Minqar District

Table 12: The relationship of physical features with soil depth and salinity of in the Dakhla-Abu Minqar District

P No.	Soil depth /cm	TDS / Mohs/cm	Alkalinity	Lime %	Gypsum%	Gavel %
1	0-30	3.08	8.4	5.9	0.03	2.5
	30-90	15.71	7.8	14.2	1.20	4.6
	90-120	15.13	7.8	10.6	1.40	14.6
2	0-50	2.89	8.5	6.2	0.03	3.1
	50-100	14.2	8.1	16.4	0.03	15.3
	100-130	13.4	8.2	11.6	1.40	16.2
3	0-50	3.12	8.4	8.6	0.03	6.8
	50-110	14.4	7.7	18.3	1.60	18.2
4	0-55	3.91	8.6	6.5	0.03	4.2
	55-110	23	7.8	19.2	1.60	6.9
	110-130	24.1	7.6	10.5	0.03	18.5
5	0--50	2.6	8.1	4.6	0.03	2.3
	50-100	13.2	7.8	19.5	5.60	16.6
6	0-25	3.41	8.6	6.2	0.03	5.6
	25-50	12.35	7.9	18.9	1.20	19.1
7	0-30	4.19	8.5	6	0.03	8.6
	30-60	6.63	8.3	19.2	2.00	18
8	0-40	3.6	8.4	6.4	0.03	8
	40-80	13.2	7.9	20.8	1.00	12.6
	80-120	8.2	8.3	18.2	1.70	14.8
9	0-35	4.6	8.4	20.1	2.00	12.8
10	0-45	8.07	7.8	19.6	3.10	16.2
11	0--50	3.2	8.2	6.8	0.03	5.3
	50-100	4.1	8.4	18.2	0.03	8.2
	100-120	7.6	7.9	17.6	1.60	16.8
12	0--35	5.7	7.9	15.6	2.00	11.9
13	0-30	4.8	7.9	18.9	1.30	18.6
14	0-50	2.68	8.3	7.6	0.03	4.6
	50-100	3.55	8.4	8.9	0.03	14.2
	100-150	3.17	8.5	18.4	2.00	18
15	0-50	3.28	8.4	10.2	0.03	6.2
	50-100	21.3	7.8	19.6	1.60	18.2
16	0-30	8.9	7.9	22	2.40	8.8
17	0-20	10.2	7.8	20.6	4.60	8.6
	0-25	5.7	8.4	21.6	5.00	10.2
	25-75	12.6	8.2	24.5	1.60	5.6
	75-130	14.8	8.1	28.3	2.10	10.2
18	0-35	10.2	7.9	25.2	2.00	11.5
19	0--25	4.3	8.4	20.1	3.10	15
	25-45	8.9	8.2	24.3	4.00	14.2

20	0-30	2.4	8.1	21	2.00	5.9
	30-60	5.8	8.2	24	3.60	11.2
	60-90	15.2	7.8	16.9	2.10	6.8
21	0-25	4.89	8.4	18.6	4.00	10.2
	25-55	23.4	7.8	20.8	2.60	12.3
22	0-35	16.52	7.9	22.6	3.60	16.5
	35-90	36.2	7.8	18.6	2.20	9
23	0-30	3.71	8.5	12.6	4.20	15.2
	30-60	7.31	8.3	23.5	2.00	18.6
24	0-35	4.2	8.2	21.2	1.80	14.3
	35-85	7.8	8.1	22.3	1.20	19.2
25	0-30	3.98	8.4	6.5	2.00	12
	30-80	8.72	7.9	8.6	1.20	15.6
	80-150	6.4	8	18.2	3.00	14.2
26	0-30	2.11	8.3	13.2	2.60	16.2
	30-100	7.35	8	16.2	1.80	12.3
	100-150	6.63	8.1	19.6	3.20	8.9
27	0-60	9.12	7.9	20.8	3.40	15.6
28	0-35	3.16	8.4	25.3	4.00	10.9
29	0-40	50.8	7.6	14.6	2.60	16
30	0-25	32.6	7.8	15.6	2.20	10.2
31	0-20	14.2	7.9	19.2	2.10	11
32	0-45	4.58	8.4	14.2	2.60	15.6
	45-90	39.8	7.8	18.9	1.40	8.2

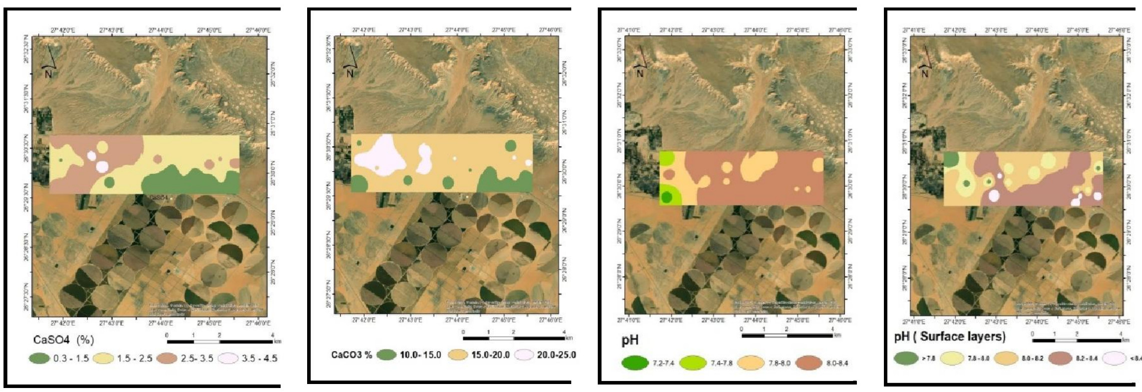

Fig. 13: Distribution maps of pH & Lime and gypsum on in the Dakhla-Abu Minqar District

Relationship between soil fertility elements with organic matters

All lands are poor in their level of nutrients and organic matter and need intensive addition of organic matter to improve texture, construction and fertility status. Levels of rare nutrients are weak in some and low in others. As a result of the high soil reaction number (pH), the plant may not benefit, notwithstanding the geological composition of the area, especially in low lands in the north with a proportion of mud and the girl child, but prefer to add organic matter, agricultural plaster and good management to overcome salinity problems, as well as to take advantage of nutrients. As a result of poor soil properties in some lands especially shallow, very shallow and high in salts, soil priorities must be used for crops. The average Fe content in soil is between 1.50 to 15 ppm. It may be due to the interaction (dissolution and leaching) between polluted groundwater and soil bedrocks. Also, the average Mn content in soil is between 0.7 to 6 ppm. It may be due to the interaction (dissolution and leaching) between polluted groundwater and soil bedrocks (Table.13).

Table 13: Soil minor elements with organic matters in In the Dakhla-Abu Minqar District

P No.	O.M %	Fertility Elements /ppm			Available Soil Nutrient /ppm				
		N	P	K	Zn	Mn	Fe	Cu	Ni
1	0.12	18.30	3.00	26.00	0.71	2.96	3.33	0.38	0.08
2	0.11	15.00	2.30	19.00	0.54	1.98	13.09	0.35	0.08
3	0.12	33.30	2.30	37.50	0.54	2.03	2.16	0.98	0.08
4	0.09	25.00	1.60	32.00	0.54	1.37	1.95	0.64	0.10
5	0.12	18.00	3.00	32.00	0.51	1.73	1.97	0.33	0.07
6	0.14	21.70	1.90	28.00	0.50	0.70	1.96	0.19	0.05

7	0.12	18.30	2.50	34.00	0.56	2.42	2.62	0.33	0.07
8	0.11	20.00	1.80	31.00	0.43	0.81	1.66	0.20	0.05
9	0.12	28.30	2.40	32.00	2.52	5.29	3.28	0.86	0.13
10	0.13	23.30	2.20	31.00	0.75	1.40	2.23	0.27	0.09
11	0.14	16.70	3.00	38.00	1.90	4.78	4.77	0.77	0.11
12	0.90	11.70	2.30	25.00	2.43	6.53	4.59	1.14	0.16
13	0.90	15.00	3.00	36.00	0.56	0.82	1.63	0.17	0.06
14	0.01	33.30	2.21	69.50	1.57	2.54	11.47	0.35	0.09
15	0.12	16.70	2.79	40.00	0.71	2.40	6.07	0.65	0.09
16	0.13	16.70	2.79	40.00	0.71	2.40	6.07	0.65	0.09
17	0.18	28.30	1.59	20.00	0.87	2.22	5.48	0.65	0.12
17-	0.19	43.30	5.08	170.00	0.51	4.25	2.46	0.43	0.07
18	0.14	26.70	1.83	57.00	2.01	6.42	6.82	2.26	0.56
19	0.13	31.70	2.43	18.00	0.52	2.58	6.88	0.47	0.07
20	0.15	40.00	1.46	15.00	0.57	2.24	5.86	0.68	0.08
21	0.18	55.00	3.08	12.50	1.21	4.03	15.57	0.88	0.10
22	0.16	41.70	2.18	15.00	0.73	1.94	4.66	0.44	0.06
23	0.18	20.00	4.68	32.50	1.06	7.47	8.02	0.60	0.19
24	0.19	38.30	12.80	12.50	0.56	3.18	5.52	0.50	0.12
25	0.12	18.30	3.00	25.00	0.45	3.20	2.15	0.22	0.08
26	0.14	25.00	2.40	56.00	0.41	0.94	2.03	0.27	0.07
27	0.16	16.70	3.00	32.00	0.54	0.95	2.06	0.20	0.06
28	0.17	21.70	1.80	32.00	0.85	1.12	2.61	0.25	0.07
29	0.33	38.30	0.97	25.00	0.91	3.96	8.15	0.69	0.10
30	0.17	48.30	1.18	23.50	1.11	3.09	7.05	0.53	0.09
31	0.15	35.00	4.20	23.00	0.68	3.47	8.05	0.49	0.08
32	0.12	15.00	2.10	23.00	0.49	1.00	2.08	0.17	0.05

Suitability of agriculture crops according soil and water quality

The results indicate that the area under consideration has a good potential to produce field crops under irrigation, provided that the water requirements are met. Nine crops were elected to assess their suitability for agriculture, namely alfalfa, wheat, maize, faba-bean, sunflower, watermelon, citrus date palm and olive. These crops are most suitable for arid and semi-arid soils. The current land suitability for different crops produced by ASLE model showed that about 60 % of the studied area is moderately suitable (S2) for Wheat. Crops such as: watermelon, alfalfa, maize, sunflower, and faba-bean are moderately suitable, marginally suitable, conditionally suitable and potentially suitable to be grown in this area (Figures 10). The main limitations are moderate to severe fertility limitations of the study area, soil depth and coarse texture. The coarse texture, shallow depth, and salinity of the soils in some soil profiles are the main limiting factors for growing crops especially fruit trees. The accumulation of salts in the crop's root zone can lower the amount of water present at the roots, posing a risk to the crop's health. Every now and then, the amount of reduced water that is available reaches levels that are detrimental to crop productivity. The slower rate of plant growth leads to the emergence of drought-like symptoms when this water pressure is increased (Ayers *et al.,* 1985). Robert S. High salinity in the water (or soil solution) results in a high osmotic potential. Certain salts can burn and or flag plant roots, which can be harmful (Figure.14). Certain metals' elevated concentrations may interfere with other micronutrients' proportionate availability and plant absorption. Because of how ionic solute concentrations functioned to classify groundwater based on salinity hazard into these categories, it is closely related to total dissolved solids (TDS); different crops could use it with varying results. Plant productivity decreased as a result of low levels of organic matter and nutrients, rising soil and water salinity in some locations, and other factors. As a result, some suggestions call for the use of new, technological fertilizers as alternatives that produce effective management outcomes. There some limitations natural or localize that hinder agriculture: In certain areas, fresh water with low salinity levels is required for soil washing. Added fertilizers for agriculture (organic fertilizers). Using foliar fertilizers is necessary to prevent high soil salinity, alkalinity, and hard soil texture. Outstanding agricultural management across all processes.

Fig. 14: Land Suitability for different crops on in the Dakhla-Abu Minqar District

Conclusion and Recommendation

Titania coated cobalt ferrite nanocomposite (TCFN) was prepared by sol gel method and utilized for the removal of Fe (II) and Mn (II) ions from polluted groundwater. Several characterization techniques, such as, FTIR, XRD, VSM, EDX, SEM, particle size distribution and BET, were applied to have a full information about the chemical composition and morphology of the prepared TCFN. The characterization studies provided useful information about the morphology of the nanocomposite and validated its formation. The best adsorption conditions for Fe (II) and Mn (II) ions were found using the batch adsorption method. The results from the characterization study confirmed the formation of the synthetized nanocomposite. The adsorption of Fe (II) and Mn (II) ions on the synthetized TCFN nanocomposite were investigated. The Optimal conditions of removal iron ion by synthesized TiO_2-Cobalt ferrite nanocomposite were Nanocomposite dosage 0.3 g/l; Contact time: 20 min.; Temp.: 45oC; PH: 6.0. Maximum adsorption capacities of 174 and 156 mg/g were achieved for Fe (II) and Mn (II) ions, respectively. Also, optimal conditions of removal iron ion by synthesized TiO_2-Cobalt ferrite nanocomposite was Nanocomposite dosage: 0.3 g/l; Contact time: 20 min.; Temp.: 45oC; PH: 5.0. Based on its remarkable adsorption capacity, fast kinetic and reusability, the prepared Titania coated cobalt ferrite nanocomposite could be considered as an outstanding adsorbent for polluted groundwater treatment. In the present study, an attempt has been made to treat the polluted groundwater around target area and relationship with soil profiles and suitability of agriculture plants. Chemical oxygen dissolved concentration varied and this data in permissible limit for good agriculture irrigation. The total nitrogen and total phosphorous were in a permissible limit. The increasing of soil salinity in some areas and also poorly organic matters & nutrients led to decreasing of plant productivity. Final land capability class has five classes which are good (C2) to Non-agriculture (C6), the main limitations were affected on land productivity are soil salinity, alkalinity and soil texture. While land suitability for main crops such as wheat, sunflower, maize, date palm and Olive were ranged from highly suitable (S1) to actually unsuitable (NS2), and main factors for decrees land productivity were soil depth , soil salinity, soil alkalinity, drainage and soil texture. So that, some recommendations need to use as alternatives new technological fertilizers that achieving good management results. Such as some area we need to soil washing by fresh water that had low salinity values. Addition of agriculture fertilizers (organic fertilizers) & Depending on foliar fertilizers to avoid alkalinity & high soil salinity and hardness texture of soil and Excellent agriculture managements for all process. Fertilizer is added in quantities that reduce the effect of calcium carbonate, knowing that the presence of calcium carbonate with sand and mixing, especially sectors from 1-8 as well as sector 14, is a good advantage for the soil. Conducting washing operations to wash excess salts in the soil by adding treated water that allows the dissolution of salts to keep the water running downwards with the availability of suitable ventilation to supply the ground with carbon dioxide to reduce pH soil. To focus on chemical fertilizer contains a high sulfur ratio and excludes fertilizer containing chlorine. Focus on fertilizer chemical soluble (fertilizer soluble) with acidic effect in the soil where it helps to lower pH soil which helps to free phosphorus and other nutrients.

Reference

Abdel Aziz, W., 1968. Geology of some Cretaceous and Eocene deposits in Farafra Oasis. M. Sc. Thesis, Fac. of Sci., Ain Shams Univ., Cairo. Abstract) Adv. Res., 7: 403-412.

Abdulhady, Y.A.M., N.S. Shahat and F.M.S. El-Dars, 2021. Int. J. Environ. Anal. Chem., 1. doi:10.1080/03067319.2021.2003348.

Aghrich, K., 2020. Experimental and first-principles study of the origin of the magnetic properties of $CoFe_2O_4$ spinel ferrite. Appl. Phys. A: Mater. Sci. Process., 126, 940, DOI: 10.1007/s00339-020-04114-z

Ahmad, Z., 2016. Structural and complex impedance spectroscopic studies of Mg-substituted $CoFe_2O_4$. Ceram. Int., 42: 18271– 18282, DOI: 10.1016/j.ceramint.2016.08.154

Ali, M.T., 2004. Evaluation of groundwater resources of El Shiekh Marzouk area at Farafra Oasis in the western desert of Egypt. Ph. D. Thesis, Geol. Dep., Fac. of Sci., Menoufiya Univ., Egypt.

Almessiere, M.A. et al., 2020. Impact of Tm3+ and Tb3+ rare earth cations substitution on the structure and magnetic parameters of Co-Ni nanospinel ferrite. Nanomaterials , 10, 2384, DOI: 10.3390/nano10122384.

Amadi P.A., C.O. Ofoegbu and T. Morrison, 1989. Hydrogeochemical Assessment of Groundwater Quality in parts of the Niger Delta, Nigeria, Environmental Geol. Water Science, 14(3):195-202.

Amiri, S., and H. Shokrollahi, 2013. The role of cobalt ferrite magnetic nanoparticles in medical science. Mater. Sci. Eng. C, 33: 1– 8, DOI: 10.1016/j.msec.2012.09.003

Apodaca, L.E., B.B. Jeffrey, and C.S. Michelle, 2002. Water quality in shallow alluvial aquifers, Upper Colorado River Basin, Colorado, Journal of American Water Research Association, 38(1):133-143.

Ayers, R.S. and D.W. West cot, 1985. Water quality for agriculture. FAO Irrigation and Drainage, Paper 29, Food and Agriculture Organization, Rome.

Barakat, M.G. and M.L. Abdel Hamid, 1974. Subsurface geology of Farafra Oasis, Western Desert, Eg. J. Geol., 17 (2): 97-110.

Braul, L., 1998. Treating High Iron, Manganese, Sulfate, and Sodium Levels. Prairie Water News. 6 (1).

Cetin, M., and H. Ozcan, 1999. Problems encountered in the irrigated and non-irrigated areas of the Lower Seyhan Plain and recommendations for solution: a case study. Tr. J. Agric. For. 23 (Suppl. 1): 207 – 217. (Turkish, with English

Chaudhary P., L. Ahamad, A. Chaudhary, G. Kumar, W. Chen and S. Chen, 2023. J. Environ. Chem. Eng. 11: 109591. doi:10.1016/j.jece.2023.109591.

Chen, X., Q. Liang, W. Gao, J. Liu, Z. Zhao, M. Yu, C. Jiang and J. Hu, 2023. J. Water Process Eng. 54: 104032. doi:10.1016/j.jwpe.2023.104032.

Clark, G.A., and A.G. Smajstrla, 2002. Treating Irrigation Systems with Chlorine. CIR1039, Fla. Coop. Ext. Ser., Univ. Fla., Gainesville.

Clemens, M., G. Khurelbaatar, R. Merz, C. Siebert, M.V. Afferden, and T. Rödiger, 2020. Groundwater protection under water scarcity; from regional risk assessment to local wastewater treatment solutions in Jordan. Sci. Total Environ., 706: 136066.

Earth System Sciences, 17: 1493-1501. https://doi.org/10.5194/hess-17-1493-2013

El Bastawesy, M., A.R. Ramadan, A. Faid, and M. El Osta, 2013. Assessment of Waterlogging in Agricultural Mega Projects in the Closed Drainage Basins of the Western Desert of Egypt. Hydrology and

El- Maghrabi, H.H., A.A. Younes, A.R. Salem, K. Rabie and E. El-Shereafy, 2019. J. Hazard. Mater. 378: 120703 . doi:10.1016/j.jhazmat.2019.05.096.

Elı'as, O., V. MarcosI, G. Eliana Urreta, E. Silvia, and P. Silvia, 2023. Journal of Magnetism and Magnetic Materials 322, 3438–3442 (2010) Eng. 11: 109591. doi:10.1016/j.jece.2023.109591.

El-Sayed M.H. and Y.A.M. Abdulhady, 2015. Egypt. J. Desert Res. 65: 81. doi:10.21608/ejdr. 2015.5802.

Foster, S.S.D. and P.J. Chitlon, 2003. Groundwater: the processes and global significance of aquifer degradation phil trans: R.soc. Land .B 358, 1957- 1972. doi: 1098/rstb2003.

Gherca, D., N. Cornei, O. Mentré, H. Kabbour, S. Daviero-Minaud, and A. Pui, 2013. In situ surface treatment of nanocrystalline MFe2O4 (M = Co, Mg, Mn, Ni) spinel ferrites using linseed oil. Appl. Surf. Sci., 287:490–498. https://doi.org/10.1016/j.apsusc.2013.10.018

Hassan, M.R., and M.I. Aly, 2021. Adsorption studies of Eu(III) ions from aqueous solutions by a synthesized copper magnetic ferrite nanoparticles as low-cost adsorbent. J. Mater. Sci., 32:19248–19263. https://doi.org/10.1007/s10854-021-06445-w

Hossain, M.S.I., M.K.R. Sarker, F. Khan, A. Khan, M. Kamruzza, and M.M. Rahman, 2018. Structural, magnetic and electrical properties of sol–gel derived cobalt ferrite nanoparticles. Appl. Phys. A. 124:608. https://hal-amu.archives-ouvertes.fr/hal-02366403

Ishaq, K., 2017. Characterization and antibacterial activity of nickel ferrite doped α-alumina nanoparticle. Eng. Sci. Technol. an Int. J., 20: 563– 569, DOI: 10.1016/j.jestch.2016.12.008

Keesari, T., U.P. Kulkarni, P. Deodhar, P.S. Ramanjaneyulu, A.K. Sanjukta, and U.S. Kumar, 2014. Geochemical characterization of groundwater from an arid region in India. Environ. Earth Sci., 71(11): 4869-4888

Kefeni, K.K., B.B. Mamba, and T.A.M. Msagati, 2017. Application of spinel ferrite nanoparticles in water and wastewater treatment: a review. Sep Purif. Technol., 13872:39422. https://doi.org/10.1016/j.seppur.2017.07.015

Kumar, M., H.S. Dosanjh, J. Singh, K. Monir, and H. Singh, 2019. Review on magnetic nano ferrites and their composites as an alternative in Waste Water Treatment: synthesis, modifications and applications. Environ. Sci. Water Res. Technol., 6:491–514. https://doi.org/10.1039/C9EW00858F

Kumar, S., R.R. Nair, P.B. Pillai, S.N. Gupta, M.A.R. Iyengar and A.K. Sood, 2014. ACS Appl. Mater. Interfaces 6, 17426–17436. Doi:10.1021/am504826q.

Langmuir, I., 1918. "Part II". The Research Laboratory of the General Electric Company: 1848.

Lin H., M. Zhou, B. Li and Y. Dong, 2023. Int. Biodeterior. Biodegr. 178: 105544. doi:10.1016/j. ibiod.2022.105544.

Lippens, B.C. and J.H. de Boer, 1965. J. Catal. 4, 319.

Liu, A.R., S.M. Wang, Y.R. Zhao and Z. Zhen, 2006. Mater. Chem. Phys. 99, 131. doi:10.1016/j. matchemphys.2005.10.003.

Liu, G., Y. Wang and R. Hong, 2010. Adv. Powder Technol. 2, 461. doi:10.1016/j.apt.2010. 01.008.

Llamas, M.R. and P. Martinez-Santos, 2005. Intensive groundwater use: Silent revolution and potential source of social conflicts. J. Water Resour. Plan. Manag.

MacBratney, A.B., and R. Webster, 1986. Choosing functions for semi-variograms of soil properties and fitting them to sampling estimates. J. Soil Sci. 37: 617 – 639.

Mahdavi, M., F. Namvar, M.B. Ahmad and R. Mohamad, 2007. Moecules 18: 5954. doi:10.3390/ molecules18055954.

Mahmoodi, N.M.M., A. Taghizadeh, and M. Taghizadeh, 2018. Mesoporous activated carbons of low-cost agricultural bio-wastes with high adsorption capacity: preparation and artificial neural network modeling of dye removal from single and multicomponent (binary and ternary) systems. J. Mol. Liq. 269:217–228. https://doi.org/10.1016/j.molliq.2018.07.108

Miyah, Y., A. Lahrichi, M. Idrissi, S. Boujraf, H. Taouda and F. Zerrouq, 2017. J. Assoc. Arab Univ. Basic Appl. Sci. 23, 20. doi:10.1016/j.jaubas.2016.06.001.

Mohamed, M.A., F. Ali Abdel-Motelib, M. Akram, and Abu Salem, Hend Saeed, 2021. Hydrogeological Characteristics of the North Eastern Part of El Farafra Oasis, Western Desert, Egypt. Egypt. J. Geo. 65: 13-26.

Munawar, T., 2021. Synthesis, characterization, and antibacterial study of novel Mg0.9Cr0.05M0.05O (M = Co, Ag, Ni) nanocrystals. Phys. B Condens. Matter , 602, 412555. DOI: 10.1016/j.physb.2020.412555

Nakayama, F.S., B.J. Boman, and D.J. Pitts, 2005. Maintenance. In Microirrigation for Crop Production. Accessed on 16, June.

Naseem, T. and T. Durrani, 2021. Environ. Chem. Ecotoxicol. 3: 59–75. doi:10.1016/j.enceco. 2020.12.001.

Nwankwoala H.O., E.V. Okeke and S.C. Okereke, 2007. Groundwater quality in parts of Port Harcourt, Nigeria: An overview, trends and concerns, International Journal of Biotechnology and Allied Sciences, 2(3): 282 – 289.

Omar, M.M. and A.M.A. Moussa, 2016. Water management in Egypt for facing the future challenges, J.

Pan, S., J. Shen, Z. Deng, X. Zhang B. Pan, and J. Hazard, 2022. Mater. 423 (Part B, 5): 127158. doi:10.1016/j.jhazmat.2021.127158.

Pandey A., A. Kalamdhad and Y.C. Sharm, 2023. Environ. Nanotechnol. Monit. Manage. 20, 100791. doi:10.1016/j.enmm.2023.100791.

Porter, D., T. Marek, T. Howell, and L. New, 2005. The Texas High Plains Evapotranspiration Network (TXHPET) User Manual. AREC Publication 05-37.

Re, V. and G.M. Zuppi, 2011. Influence of precipitation and deep saline groundwater on the hydrological systems of Mediterranean coastal plains: a general overview. Hydrol. Sci. J., 56 (6): 966-980.

Salem, A.A.A., 2002. Hydrogeological studies on the Nubia Sandstone Aquifer in Bahariya and Farafra depressions, Western Desert, Egypt. Ph.D. Thesis, Geol. Dep., Fac. of Sci., Ain Shams Univ., Cairo.

Sharma, B., P.K. Boruah, A. Yadav and M.R. Das, 2018. J. Environ. Chem. Eng. 6, 134. doi:10. 1016/j.jece.2017.11.025.

Shirsath, S.E., X. Liu, Y. Yasukawa, S. Li, and A. Morisako, 2016. Switching of magnetic easy-axis using crystal orientation for large perpendicular coercivity in CoFe2O4 thin film. Sci. Rep. , 6, 30074, DOI: 10.1038/srep30074

Shrestha, B.B., M. Kokh and J.B. Karki, 2016. Mapping of invasive alien plant species in Tarai Arc Landscape (TAL) and ChitwanAnnapurna Landscape (CHAL), Nepal. Unpublished research report submitted to National Trust for Nature Conservation (NTNC), Kathmandu, Nepa.

Song, W., X. Zhang, L. Zhang, Z. Yu, X. Li, Y. Li, Y. Cui, Y. Zhao and L. Yan, 2023. J. Mol. Liq. 375, 121386 . doi:10.1016/j.molliq.2023.121386.

Udom, G.J., J.O. Etu- Efeotor and E.O. Esu, 1999. Hydrochemical evaluation of groundwater in parts of Port Harcourt and Tai-Eleme Local Government Area, Rivers State., Global Journal of Pure and Applied Sciences, (5):546 – 552.

USSL. 1954. Diagnosis and improvement of saline and alkali soils, USDA Hand waters, 3rd edition US Geol. Survey, water supply paper 2254, scientific pub.

Velhal, N.B., N.D. Patil, A.R. Shelke, N. G. Deshpande, and V. R. Puri, 2015. Structural, dielectric and magnetic properties of nickel substituted cobalt ferrite nanoparticles: Effect of nickel concentration. AIP Adv., 5: 097166, DOI: 10.1063/1.4931908

Wang, G. and G. Cheng, 1999. Water resource development and its influence on the environment in arid areas of China-the case of the Hei River basin, J. Arid Environ., 43: 121-131

Xiao, B., J. Jia, W. Wang, B. Zhang, H. Ming, S. Ma, Y. Kang and M. Zhao, 2023. J. Hazard. Mater. Adv.10: 100254 . doi:10.1016/j.hazadv.2023.100254.

Yadav, N., S. Singh, O. Saini and S. Srivastava, 2022. Environ. Nanotechnol. Monit. Manag. 18:100757. doi:10.1016/j.enmm.2022.100757.

Yan, L., X. Yang, H. Zeng, Y. Zhao, Y. Li, X. He, J. Ma and L. Shao, 2023. J. Memb. Sci. 668: 121243 . doi:10.1016/j.memsci.2022.121243.

Younes, A.A., A.M. Masoud and M.H. Taha, 2021. Int. J. Environ. Anal. Chem., 1–14. doi:10.1080/03067319.2021.2003348.

Zhang, Y., J. Luo, H. Zhang, T. Li, H. Xu, Y. Sun, X. Gu, X. Hu and B. Gao, 2022. Sci. Total Environ. 852: 158201 .doi:10.1016/j.scitotenv.2022.158201.